Final version available at: http://www.sciencedirect.com/science/article/pii/S0277379116302633

Sources, transport and deposition of terrestrial organic material: a case study from southwestern Africa

Nicole Herrmann [a,*], Arnoud Boom [b], Andrew S. Carr [b], Brian M. Chase [c], Robyn Granger [d], Annette Hahn [a], Matthias Zabel [a], Enno Schefuß [a]

[a] MARUM – Center for Marine Environmental Sciences, University of Bremen, Leobener Straße, Bremen, Germany

[b] Department of Geography, University of Leicester, University Road, Leicester LE1 7RH, United Kingdom

[c] Centre National de Recherche Scientifique, UMR 5554, Institute des Sciences de l'Evolution de Montpellier, Département Paléoenvironnements, Université Montpellier, Bat.22, CC061, Place Eugène Bataillon, 34095, Montpellier, Cedex 5, France

[d] Department of Environmental and Geographical Science, University of Cape Town, Rondebosch 7701, South Africa

*** Corresponding author**

Email: nherrmann@marum.de

Abstract

Southwestern Africa's coastal marine mudbelt, a prominent Holocene sediment package, provides a valuable archive for reconstructing terrestrial palaeoclimates on the adjacent continent. While the origin of terrestrial inorganic material has been intensively studied, the sources of terrigenous organic material deposited in the mudbelt are yet unclear. In this study, plant wax derived *n*-alkanes and their compound-specific $\delta^{13}C$ in

soils, flood deposits and suspension loads from regional fluvial systems and marine sediments are analysed to characterize the origin of terrestrial organic material in the southwest African mudbelt. Soils from different biomes in the catchments of the Orange River and small west coast rivers show on average distinct *n*-alkane distributions and compound-specific $\delta^{13}C$ values reflecting biome-specific vegetation types, most notably the winter rainfall associated Fynbos Biome of the southwestern Cape. In the fluvial sediment samples from the Orange River, changes in the *n*-alkane distributions and compound-specific $\delta^{13}C$ compositions reveal an overprint by local vegetation along the river's course. The smaller west coast rivers show distinct signals, reflecting their small catchment areas and particular vegetation communities. Marine surface sediments spanning a transect from the northern mudbelt (29°S) to St. Helena Bay (33°S) reveal subtle, but spatially coherent, changes in *n*-alkane distributions and compound-specific $\delta^{13}C$, indicating the influence of Orange River sediments in the northern mudbelt, the increasing importance of terrigenous input from the adjacent western coastal biomes in the central mudbelt, and contributions from the Fynbos Biome to the southern mudbelt. These findings indicate the different sources of terrestrial organic material deposited in the mudbelt, and highlight the potential the mudbelt has to preserve evidence of environmental change from the adjacent continent.

Keywords

South Africa, compound-specific carbon isotopes, *n*-alkanes, marine surface sediments, soils

1 Introduction

Coastal marine sediments serve as important archives for palaeoenvironmental investigations (e.g. Just et al., 2014; Rommerskirchen et al., 2006a). However, provenance, transport and sedimentation processes of the investigated tracers must be considered to reconstruct palaeoclimatic changes on the adjacent continent. In numerous studies of modern river systems the origin and transport processes of the source signals are shown to be complex. Overprinting of the transported source signals in river sediments on their way to the sedimentary archives (e.g. Bouchez et al., 2014; Galy et al., 2011; Garzanti et al., 2015; Hemingway et al., 2016) and in some contexts, a decoupling of inorganic and organic material provenance (e.g. Just et al., 2014; Schefuß et al., 2011) complicate interpretations. Additionally, changes in sedimentary provenance through time should not be neglected (e.g. Bentley et al., 2016; Leithold et al., 2016; Woodward et al., 2015). Thus, determining the provenance of signal carriers in coastal marine sediments is a key to understand palaeoenvironmental changes. For such an archive, the southwestern Africa's mudbelt, a terrigenous mud deposit of Holocene age, is a good example (Herbert and Compton, 2007; Mabote et al., 1997; Meadows et al., 2002). While the origin and transport of inorganic material has been intensively studied (Birch, 1977; Compton et al., 2010; Hahn et al., 2015; Mabote et al., 1997; Rogers and Rau, 2006; Weldeab et al., 2013), this study is aiming to refine our understanding of organic matter delivery to this archive.

Fluvial and aeolian transport deposits large amounts of terrestrial organic matter (~ 430 Tg organic carbon (OC) year^{-1} and 60 Tg OC year^{-1}, respectively) to the ocean sediments (e.g. Jurado et al., 2008; Schlünz and Schneider, 2000; Simoneit, 1986). The type, amount and isotopic composition of terrestrial organic matter carries information

about continental environmental conditions making it a potential means of reconstructing past climates (e.g. Meyers, 1997). In particular, stable carbon isotope compositions ($\delta^{13}C$) of terrestrial organic carbon have been used to identify vegetation sources and changes thereof (e.g. Meyers, 1994; Prahl et al., 1994). However, as the total organic matter in sedimentary archives is derived from both terrestrial and aquatic sources, the significance of measurements from bulk samples is difficult to interpret (e.g. Meyers, 1994). This can be addressed though the isolation and measurement of specific lipids, such as plant epicuticular waxes, which are solely produced by terrestrial higher plants in continental environments and are preserved over geological timescales (e.g. Aichner et al., 2010; Collins et al., 2013; Kuechler et al., 2013; Meyers and Ishiwatari, 1993; Rommerskirchen et al., 2006a, 2003; Schefuß et al., 2011).

A significant component of epicuticular waxes are long-chain *n*-alkanes with chain lengths between 21 and 37 carbon atoms and an odd-over-even carbon number predominance (Eglinton and Hamilton, 1967; Kolattukudy, 1970). Many studies suggest that vegetation type and/or climate determine the production and chain length distribution of leaf wax *n*-alkanes (Bush and McInerney, 2015, 2013; Carr et al., 2014; Meyers and Ishiwatari, 1993; Rao et al., 2011; Vogts et al., 2009). For example, angiosperms and plants adapted to arid conditions generally produce higher amounts of waxes than gymnosperms (Diefendorf et al., 2011) while plants from African savannas were shown, on average, to produce longer chain *n*-alkanes than rainforest plants (Rommerskirchen et al., 2006b; Vogts et al., 2009).

The $\delta^{13}C$ composition of plant tissue differs with plant photosynthetic pathways. Leaf wax *n*-alkanes from plants using the C_3 cycle (i.e. trees, shrubs and cool season grasses) are more ^{13}C-depleted (-29‰ to -39‰ VPDB) than those from plants using the

C_4 cycle (i.e. warm season grasses; -14‰ to -26‰ VPDB) (e.g. Bi et al., 2005; Collister et al., 1994; Rommerskirchen et al., 2006b). Plants using the crassulacean acid metabolism photosynthesis (CAM; many succulent plants) are common in tropical and arid regions, and can show highly variable leaf wax $\delta^{13}C$ composition, often falling between that of C_3 and C_4 plants (e.g. Boom et al., 2014; Chikaraishi and Naraoka, 2003; Collister et al., 1994). Apart from the plant's photosynthetic pathway, the $\delta^{13}C$ of *n*-alkanes is also influenced by a variety of other factors, such as the initial $\delta^{13}C$ of the fixed CO_2 (e.g. Farquhar et al., 1989; van der Merwe and Medina, 1991) or variations in plant water-use efficiency (e.g. Ehleringer et al., 1992; Farquhar et al., 1989; Gao et al., 2015; Hou et al., 2007) with the latter most common in arid and semi-arid areas.

2 Background of the study area

2.1 Vegetation in South Africa

In the modern South African vegetation, C_3, C_4 and CAM plants are abundantly represented (Werger and Ellis, 1981). The distribution of modern biomes in South Africa generally follows the climate gradients extending eastward from the arid Desert and Succulent Karoo through the Nama Karoo, Savanna, Grassland, Thicket and Coastal Forest (Indian Coastal Belt) in the humid east and southward to the mediterranean Fynbos Biome in the Cape and the Afromontane Forest Biome of the south coast (Fig. 1) (Cowling et al., 1997; Mucina and Rutherford, 2006). The Fynbos Biome and the cool, high altitude grasslands of the Drakensberg Mountains are dominated by woody C_3 plants and C_3 grasses. The abundance of C_4 grasses increases with aridity and growing season temperature (Scott and Vogel, 2000; Vogel et al., 1978) and is highest in the interior of South Africa (Werger and Ellis, 1981). CAM plants occur throughout southern

Africa, and may become dominant in arid regions with high rainfall seasonality, such as the Succulent Karoo and western Nama Karoo biomes (Mooney et al., 1977; Werger and Ellis, 1981).

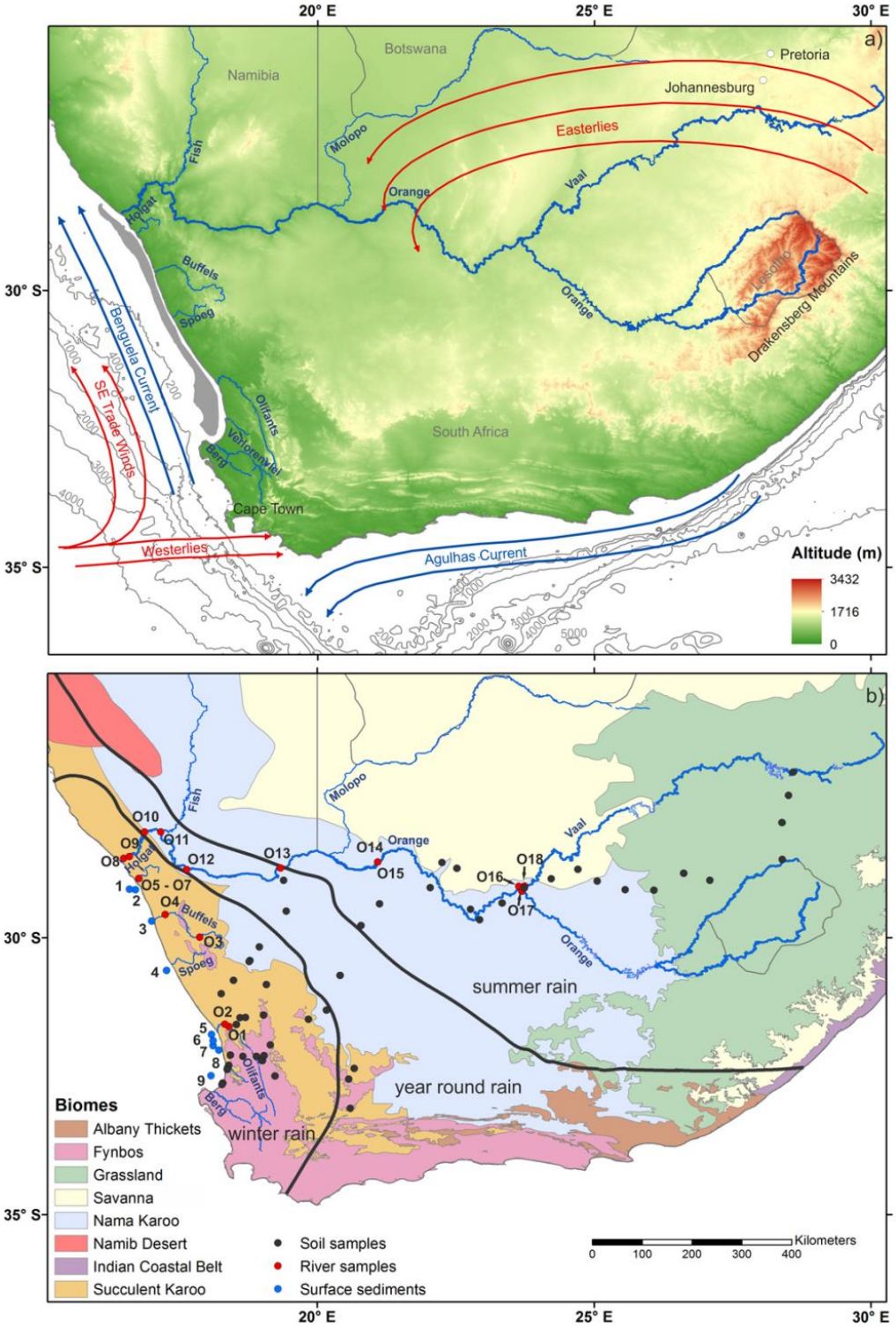

Figure 1: Overview of the main atmospheric (red arrows) and oceanic currents (blue arrows) as well as the topography and bathymetry of the study area in southern Africa (a). The shaded grey area indicates the mudbelt, grey lines on the continent indicate state borders. The lower map (b) shows the three main rainfall zones: winter rainfall zone, summer rainfall zone and year-round rainfall zone. Colours indicate modern vegetation of southern Africa (after Mucina & Rutherford, 2006; Scott et al., 2012). Dots denote the locations of soil samples (black), river samples (flood deposits and suspension, red) and marine surface samples (blue).

2.2 Hydrology in South Africa

The vegetation distribution in South Africa (Fig. 1) is largely controlled by topography and climatic conditions. The climatic conditions are driven by seasonal changes in large-scale dynamic atmospheric and oceanic circulation systems inducing a pronounced seasonality of rainfall and temperature (e.g. Tyson & Preston-Whyte, 2000). The southwestern margin of southern Africa receives most of its precipitation during the austral winter, brought by westerly winds from the Atlantic Ocean (Tyson, 1986). The southwestern part of South Africa is therefore referred to as the winter rainfall zone (WRZ), where >66% of the mean annual precipitation falls between April and September (Chase and Meadows, 2007). In contrast, much of central and eastern southern Africa receives >66% of its mean annual precipitation between October and March (Chase & Meadows, 2007) and is therefore referred to as the summer rainfall zone (SRZ). A dynamic transition zone between WRZ and SRZ receives broadly equal amounts of precipitation in the summer and winter months and is referred to as year-round rainfall zone (YRZ). Despite these spatial distinctions, the circulation systems that supply rainfall to these regions are known to interact, creating systems such as tropical-temperate troughs, which may result in large rainfall events in the continental interior (Nicholson, 1986; Tyson, 1986).

Much of the precipitation falling in South Africa drains into the Atlantic Ocean. The Orange River, the largest in South Africa, drains much of the interior, from Windhoek (22°33.57’S, 17°4.99’E), Namibia in the north to Pretoria and the Drakensberg Mountains in the east, encompassing a catchment area of almost 10^6 km^2 and currently delivering 106 x 10^6 m^3 of sediment annually (Birch et al., 1991; Compton et al., 2010) to the Atlantic Ocean from the SRZ. South of the Orange River mouth, several local

ephemeral (e.g. Holgat, Buffels, Spoeg, Verlorenvlei) and perennial (Olifants, Berg) rivers drain into the Atlantic Ocean from the WRZ. The catchments of these ephemeral rivers are small and limited to the arid/semi-arid escarpment that borders the western South African margin (Bickerton, 1981a, 1981b; Heinecken, 1981). The Olifants and Berg rivers are located in the wetter southern parts of the WRZ and also comprise relatively small catchment areas (46 x 10^3 km^2 & 7.7 x 10^3 km^2, respectively), sourced in the Cape Fold Belt Mountains (CSIR, 1988; Morant, 1984). They deliver more sediment load to the mudbelt (7.7 x 10^6 m^3) than the ephemeral rivers, but still far less than the Orange River (Birch et al., 1991; Compton and Wiltshire, 2009; Herbert and Compton, 2007).

2.3 Marine sediments offshore southwestern Africa

Offshore, the southwestern African mudbelt represents a prominent Holocene terrestrial sediment package that reaches a thickness of about 35 m near the Orange River mouth (29°S), decreasing to about 2 m near the Berg River (33°S) (Birch, 1977; Meadows et al., 2002; Rogers and Rau, 2006; Schneider et al., 2003). The thickness, accumulation rate of the sediments and their predominant terrestrial origin make the mudbelt a high-resolution archive for the investigation of Holocene environmental change (Birch, 1977; Gray, 2009; Hahn et al., 2015; Herbert and Compton, 2007; Leduc et al., 2010; Mabote et al., 1997; Weldeab et al., 2013). The Orange River is the main sediment source for the mudbelt as the mud fraction of the suspended material delivered by the Orange River is transported southwards by a poleward undercurrent (Birch et al., 1991; Mabote et al., 1997; Rogers and Bremner, 1991). Studies of the northern mudbelt have shown that the contribution of marine organic material becomes increasingly dominant further south near the Buffels River mouth (Gray et al., 2000; Mabote et al., 1997; Meadows et

al., 2002; Rogers and Rau, 2006). Further south in the central mudbelt, the importance of sediment contributions by local ephemeral west coast rivers increases (Benito et al., 2011b; Gray, 2009; Gray et al., 2000; Mabote et al., 1997). In the southern mudbelt the Olifants and Berg rivers are the dominant sediment source (Birch, 1977).

Considered in its Quaternary context, a substantial sediment deficit exists on the southern portion of the western shelf. While the Olifants, Verlorenvlei and Berg rivers currently contribute only 6% of the annual sediment load (compared with 92.7% from the Orange River), the Quaternary sediment volume of the Olifants-Berg region is 71% of that of the Orange River delta (Birch et al., 1991), indicating significant spatio-temporal variability in sedimentation regimes along the west coast. Exploring related patterns of variability for the Holocene, Herbert & Compton (2007) found a greater input of terrigenous sediments to this area during the mid- to late Holocene and therefore inferred a southward progradation of the mudbelt from the Orange River mouth.

An additional potential contribution to the mudbelt sediments is aeolian terrestrial input from the west coast by berg winds and southeast trade winds (Tyson and Preston-Whyte, 2000; Weldeab et al., 2013). While the westerly and south-westerly aeolian input south of 25°S is suggested to be low (Dupont and Wyputta, 2003; Prospero et al., 2002), inconsistencies between marine (Shi et al., 2001; Urrego et al., 2015) and terrestrial pollen records (Lim et al., in press; Scott et al., 2004, 1995), and significant changes in wind strength along the western coastal margin during the late Quaternary (Farmer et al., 2005; Pichevin et al., 2005; Stuut et al., 2002) imply that aeolian input may have been more significant in the past.

2.4 Sediment provenance

So far, little consensus exists regarding the significance and dominant sedimentary sources of the major tributaries. Several studies suggested that the terrestrial sediment transported to the Orange River mouth is largely sourced in the Karoo sedimentary rocks (upper Beaufort and Stormberg groups) and soils of the Drakensberg Mountains attributed to higher rates of weathering and erosion caused by higher rainfall in the eastern catchment (Compton and Maake, 2007; de Villiers, 2000; Le Roux, 1990; Mabote et al., 1997). In contrast, it is thought that the Vaal River transports only low concentrations of suspended sediments due to its low gradient and, since the 20th century, the construction of large dams in its upstream portion (Compton and Maake, 2007; Rooseboom and von Harmse, 1979; Schwartz, 1969). Recently Hahn et al. (2015) suggested that input to the mudbelt from other source areas, namely the catchment areas of the Molopo and the Fish River (Fig. 1), may be significant, especially during wetter phases in these sub-catchments.

Together, previous studies show a contradictory picture concerning the provenance of terrestrial material deposited in the southwestern African mudbelt. So far, most studies of mudbelt sediment provenance have focused on the mineralogical fraction (and inorganic geochemical compositions) rather than the organic fraction. Presently, little is known about the origin, transport and deposition of the terrestrial organic material in the mudbelt. In this study, we focus on characterizing the organic component of the mudbelt sediments along its entire length, from the Cape to the Orange River mouth. We use a data-set of leaf wax derived long-chain *n*-alkanes as tracers for terrestrial organic matter. We analyse their abundance, distributions and compound-specific $\delta^{13}C$ compositions in soils, flood deposits and contemporary suspension loads from regional fluvial systems and marine surface sediments, from

South African biomes, rivers and the offshore mudbelt to obtain a source-to-sink assessment. The main aims of this study are:

i) To characterize long-chain *n*-alkane distributions and compound-specific $\delta^{13}C$ compositions in the biomes within the catchments of the Orange River and the west coast rivers.

ii) To identify sources and potential overprinting effects during transport of leaf wax *n*-alkanes in suspension loads and sediments of the Orange River and the smaller west coast rivers, i.e. Buffels, Holgat and Olifants.

iii) To determine sources of terrestrial organic matter across the southwest African mudbelt and to assess the relative contributions of distinct ecoregions.

iv) To assess the palaeoenvironmental potential of plant biomarkers deposited in the mudbelt sediments.

3 Material & Methods

3.1 Sampling

Soil samples were collected in 2010, 2012 and 2013 (Fig. 1). Part of the soil sampling in the Succulent Karoo and Fynbos biomes in 2010 was carried out via a series of 10 x 10 m vegetation survey plots from which soils were collected from the upper 10 to 15 cm (soil A horizon) from four fixed locations within each plot (see Carr et al., 2013 for further information). For the other soil samples three samples from a 10-20 m radius were collected, but were not associated with detailed vegetation surveys.

Suspensions loads and most of the flood deposits from the Olifants, Buffels, Holgat and Orange rivers were collected in combusted glass jars, while some flood

deposits were stored in plastic bags. The suspension loads were retrieved by centrifuging of 100 litres of pumped river water.

For the marine surface sediments, nine multi-cores from the mudbelt off the west coast of South Africa recovered during cruise M57/1 in 2003 (Schneider et al., 2003) were sampled. The top centimetre of each core was analysed. Two multi-cores in the northern mudbelt (GeoB8331-2, GeoB8332-3) were dated earlier using $^{210}Pb_{ex}$ measurements (Leduc et al., 2010), demonstrating that the upper centimetre of both cores is not older than three years. Radiocarbon dating was performed on two multi-cores (GeoB8319-1, GeoB8322-1) in the southern mudbelt resulting in ages of 110-40 cal. yr BP between 11-14 cm (GeoB8319-1) and 630-370 cal. yr BP at 43 cm (GeoB8322-1), respectively (Taylor, 2004). Furthermore, pollen analyses of the upper three centimetres of all studied multi-cores identified neophytes (Zhao et al., 2015) introduced by the end of the 17th century in South Africa (Campbell and Moll, 1977; Richardson, 2000). The upper first centimetre of each multi-cores is thus considered to be of ‘modern’ age.

3.2 Radiocarbon dating

For some flood deposits and soil samples AMS ^{14}C analyses were performed at the Poznan Radiocarbon Laboratory on total organic carbon (TOC). Age calibration was performed using OXCAL4.2 software (Bronk Ramsey, 2009) and the atmospheric SHCal13 curve (Hogg et al., 2013).

3.3 Sample preparation and lipid extraction

Soil samples were freeze-dried at the University of Leicester and homogenized after removing root and stem pieces. Wet flood deposits, suspension loads and marine sediments were freeze dried at MARUM. Suspension loads were homogenized with a

planetary mill and flood deposits and marine sediments were homogenized by using an agate mortar and pestle.

The organic compounds were extracted from all samples using an Accelerated Solvent Extractor (ASE) at 100°C, 1000 psi for 5 minutes by using a 9:1 solvent mixture of dichloromethane (DCM) and methanol (MeOH). This extraction procedure was repeated three times for each sample. Before extraction squalane was added in known amount as internal standard. The total lipid extracts (TLEs) were concentrated using rotary evaporation and desulphurised with activated copper. Afterwards, the TLEs were separated into hexane-insoluble and hexane-soluble fractions by Na_2SO_4 column chromatography. The hexane-soluble fractions were saponified with 0.1M potassium hydroxide (KOH) in MeOH at 85°C for two hours and neutral compounds were extracted with hexane. Hydrocarbons were separated from the neutral fractions by column chromatography with silica gel (60 mesh) using hexane. Further $AgNO_3$-Si column chromatography was applied to separate the unsaturated and saturated hydrocarbon fractions using hexane.

For some soil samples urea adduction was carried out to separate *n*-alkanes from cyclic and branched hydrocarbons to gain a better compound separation for compound-specific $\delta^{13}C$ analysis. 4.5 ml hexane/DCM (2:1) and 1.5 ml urea solution (40 mg/ml in MeOH) were added to the hydrocarbon fractions and cooled at 4°C for 15 minutes. The solution was dried under nitrogen. To separate branched and cyclic hydrocarbons, hexane was added to the dried sample. After vortexing for 30 seconds the hexane was removed via pipette. The procedure was conducted three times. Straight-chain *n*-alkanes were extracted using hexane/DCM (4:1), after adding MilliQ water to dissolve the urea crystals.

Leaf wax *n*-alkane distributions for several of the soil samples were reported by Carr et al. (2014). To ensure comparability in this study all samples were re-extracted. We note that the *n*-alkane distribution data from Carr et al. (2014) are highly comparable to those obtained in this study.

3.4 Instrumental analyses and calculations

Quantification of long-chain *n*-alkanes was carried out using a ThermoFischer Scientific Focus gas chromatograph equipped with a split/splitless injector operating at 340°C and a flame ionization detector (GC-FID). For quantification an external standard was used containing *n*-alkanes between C_{18} and C_{34} in known concentrations. Based on repeated analyses of the external standard, quantification precision is 5 %. The carbon preference index (CPI) was calculated as:

$$CPI_{27-33} = 0.5 * \left[\left(\frac{C27+C29+C31+C33}{C26+C28+C30+C32}\right) + \left(\frac{C27+C29+C31+C33}{C28+C30+C32+C34}\right)\right]$$

where C_x is the concentration of the *n*-alkane with x carbon atoms.

The average chain length (ACL) of the homologues C_{27} to C_{33} was calculated as:

$$ACL_{27-33} = \frac{27*C27+29*C29+31*C31+33*C33}{C27+C29+C31+C33}$$

where C_x is the concentration of the *n*-alkane with x carbon atoms.

In several studies the ratios between individual *n*-alkanes are used as environmentally sensitive parameters (e.g. Carr et al., 2014; Schefuß et al., 2003). The ratio of the *n*-alkane homologues C_{29} and C_{31} and C_{29} and C_{33} were calculated as:

Norm31 = C31/(C29+ C31)

and

Norm33 = C33/(C29+ C33)

where C_x is the concentration of the *n*-alkane with x carbon atoms.

Compound-specific $\delta^{13}C$ analyses of *n*-alkanes were performed using a ThermoFischer Scientific Trace GC Ultra coupled to a Finnigan MAT 252 irm-MS (GC-irm-MS) via a modified GC/C III interface operated at 1000°C. The GC-irm-MS was equipped with a PTV injector operating with cold injection. Carbon isotopes where measured against calibrated CO_2 reference gas. $\delta^{13}C$ values are reported in ‰ notation against the Vienna Pee Dee Belemnite (VPDB). Duplicates of each sample were measured, with a reproducibility of 0.2‰ for the *n*-C_{29} alkane and 0.1‰ for the *n*-C_{31} alkane on average. The precision of the squalane internal standard for surface sediments, river samples and soils was 0.3‰, 0.4‰ and 0.4‰, respectively. Long-term precision and accuracy of the external *n*-alkane standard is 0.3‰ and 0‰, respectively.

4 Results

4.1 TOC ages in soil and river samples

The results of the ^{14}C measurements on bulk TOC for the soil and river samples are given in Table 1. Both soil samples (GTC9 and GTC24 from the Grassland and Savanna Biome, respectively) are of modern age whereas river samples span last 1000 years. The flood deposit O13 (Fig. 1) in the lower Orange River is of modern age while the two flood deposits O16 at the Orange-Vaal confluence and O17 (Fig. 1) in the Orange River valley upstream of the confluence span a time period of 430 ± 110 cal. yr BP and 515 ± 20 cal. yr BP, respectively. The oldest dated flood deposits include O10 at the lower reaches of the Orange River valley and O18 (Fig.1) in the Vaal River valley with ages of 1017 ± 65 and 856 ± 65 cal. yr BP respectively.

Table 1: AMS radiocarbon analyses of bulk total organic carbon (TOC) of soils and river samples from the Orange River.

	Location	Sample name	Lab. No.	Material	14C age yr BP	Cal age yr BP			Calibration data
						Median	+1σ	-1σ	
Soils									
		GTC9-1	Poz-71850	Bulk TOC	107.63 ± 0.38 pMC	post 1950			
		GTC24-3	Poz-71851	Bulk TOC	105.34 ± 0.33 pMC	post 1950			
River samples	O10	ORF25	Poz-67126	Bulk TOC	1170 ± 30	1017	1089	956	SHCal13 (Hogg et al., 2013)
	O13	ORF29T	Poz-63487	Bulk TOC	105.04 ± 0.31 pMC	post 1950			
	O18	ORF35	Poz-63486	Bulk TOC	1000 ± 70	856	926	797	SHCal13 (Hogg et al., 2013)
	O17	ORF37	Poz-67127	Bulk TOC	515 ± 30	515	542	495	SHCal13 (Hogg et al., 2013)
	O16	ORF40	Poz-63697	Bulk TOC	430 ± 70	431	529	309	SHCal13 (Hogg et al., 2013)

4.2 *n*-Alkane characteristics

In the following section the *n*-alkane characteristics are described separately for soils (source), river samples (transport) and mudbelt sediments (sink). C_x refers to the *n*-alkane with x carbon atoms. The compound-specific carbon isotope compositions are expressed as $\delta^{13}C_x$.

4.2.1 Soil samples

Long-chain *n*-alkanes were found in all soil samples with concentrations (sum of C_{25}-C_{33}) between 1 and 47 µg/g soil (see supplementary material). In general, the soil samples show a strong odd-over-even carbon number predominance with CPI_{27-33} values ranging between 2.4 and 30.2 and ACL_{27-33} ranging between 29.5 and 32.1. Differences in the *n*-alkane distributions are observed for the different biomes (Fig. 2). We found the highest relative abundance of C_{31} alkane in soils located in Succulent Karoo and Nama Karoo biomes, which showed a similar pattern. The *n*-alkane distributions for Grassland and Savanna biome soils also exhibit similarities, including the highest relative abundances of C_{31} and C_{33}. Fynbos Biome soils are distinct to some

extent with a dominance of the C_{29} and C_{31} alkanes. Highest Norm31 ratios are observed in soils of the Succulent Karoo followed by Nama Karoo, while the Grassland, Savanna and Fynbos soils show generally lower Norm31 ratios (Table 2). Norm33 ratios show a different pattern to Norm31, with highest values in soils of the Succulent Karoo followed by Savanna and Grassland soils (Table 2).

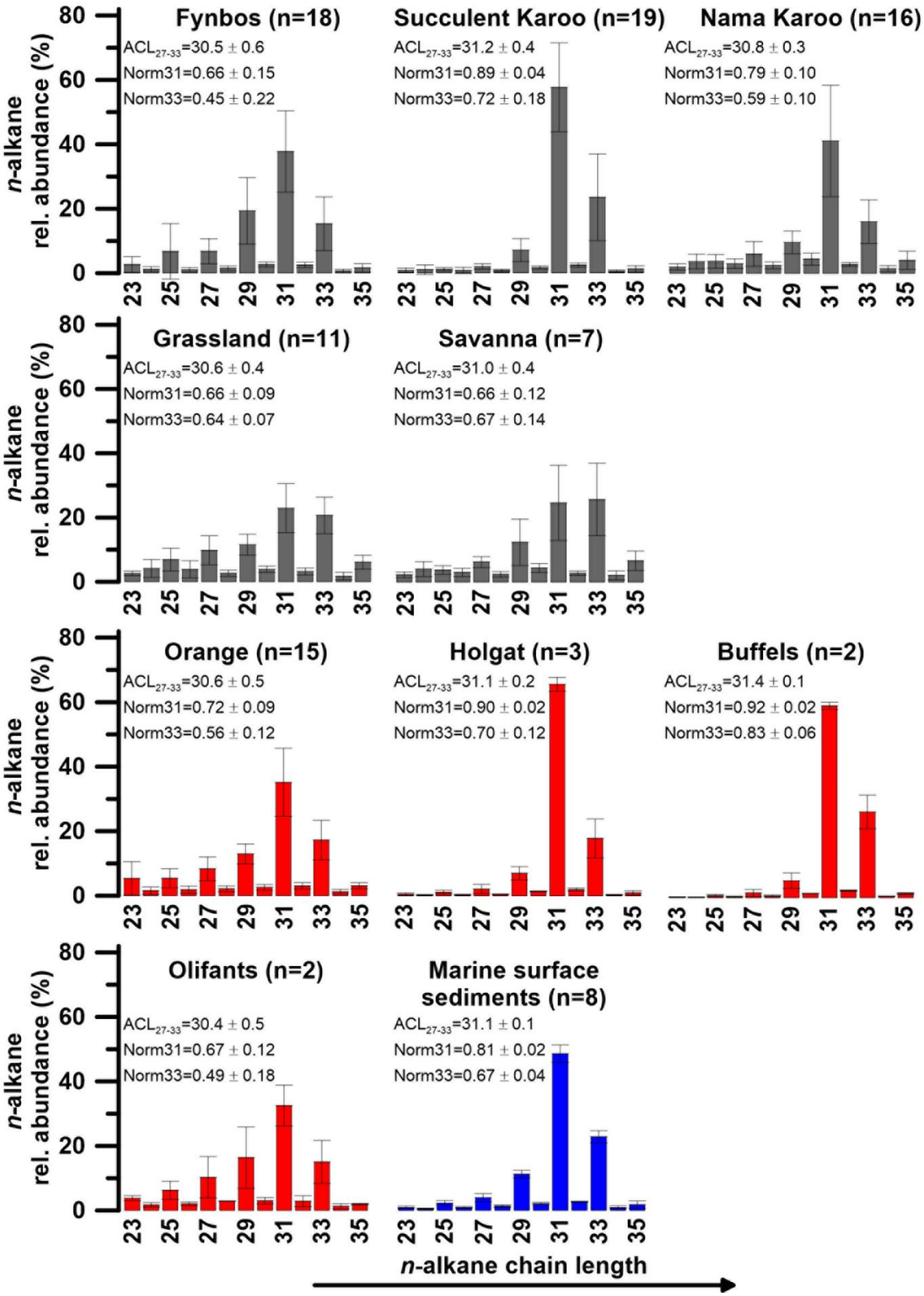

Figure 2: Averaged relative *n*-alkane distribution with standard deviation of biomes (grey), river samples (red) and marine surface sediments (blue). River samples comprise of flood deposits and suspension loads. Numbers in brackets (n) indicates the number of samples.

$\delta^{13}C$ values in soils throughout the study area cover a broad range spanning from -34.4‰ to -20.8‰ (C_{29}) and from -34.8‰ to -21.7‰ (C_{31}), respectively (Fig. 3). Lowest average $\delta^{13}C_{29}$ are observed in Fynbos soils (-32.1‰ ± 1.4‰) followed by Succulent Karoo soils (-29.8‰ ± 2.4‰) and Nama Karoo soils (-27.4‰ ± 2.7‰), whereas the highest average values are found in Savanna (-26.3‰ ± 1.8‰) and Grassland (-25.2‰ ± 3.5‰) soils (Table 2). For $\delta^{13}C_{31}$ lowest average values are found in Fynbos soils (-32.3‰ ± 1.0‰), whereas the highest values are found in Grassland soils (-25.8‰ ± 3.3‰) (Table2).

Table 2: Averaged *n*-alkane abundances, distribution parameters and compound-specific δ13C compositions of different biomes, rivers and the marine surface samples.

		Number of samples	*n*-alkane content$_{25-33}$ (µg/g sed)	ACL_{27-33}[a]	CPI_{27-33}[b]	Norm31[c]	Norm33[d]	$\delta^{13}C_{29}$ (‰ VPDB)	$\delta^{13}C_{31}$ (‰ VPDB)
Biome									
	Fynbos	18	8.5 ± 11	30.5 ± 0.6	11.0 ± 3.2	0.66 ± 0.15	0.45 ± 0.22	-32.1 ± 1.4	-32.3 ± 1.0
	Succulent Karoo	19	10 ± 8.8	31.2 ± 0.4	18.1 ± 5.8	0.89 ± 0.04	0.72 ± 0.18	-29.8 ± 2.4	-27.9 ± 2.8
	Nama Karoo	16	3.3 ± 4.0	30.8 ± 0.3	7.5 ± 4.1	0.79 ± 0.10	0.59 ± 0.10	-27.4 ± 2.7	-28.7 ± 2.7
	Savanna	7	2.2 ± 0.9	31.0 ± 0.4	6.2 ± 2.1	0.66 ± 0.12	0.67 ± 0.14	-26.3 ± 1.8	-28.1 ± 2.8
	Grassland	11	3.7 ± 1.8	30.6 ± 0.4	5.5 ± 1.6	0.66 ± 0.09	0.64 ± 0.07	-25.2 ± 3.5	-25.8 ± 3.3
Rivers									
	Olifants	2	7.4 ± 4.3	30.4 ± 0.5	7.5 ± 1.9	0.67 ± 0.12	0.49 ± 0.18	-31.0 ± 1.5	-28.2 ± 1.8
	Buffels	2	100 ± 53	31.4 ± 0.1	21.0 ± 1.0	0.92 ± 0.02	0.83 ± 0.06	n.d.	-27.1 ± 0.2
	Holgat	3	41 ± 20	31.1 ± 0.2	22.2 ± 2.0	0.90 ± 0.02	0.70 ± 0.12	-25.7 ± 0.2	-24.3 ± 0.8
	Orange	15	7.6 ± 7.1	30.6 ± 0.5	8.7 ± 2.7	0.72 ± 0.09	0.56 ± 0.12	-29.6 ± 1.4	-28.6 ± 1.7
Mudbelt		9	8.6 ± 8.5	31.1 ± 0.1	12.2 ± 1.8	0.81 ± 0.02	0.67 ± 0.04	-28.0 ± 0.5	-26.3 ± 0.4

n.d. = not determined

[a] ACL_{27-33}: averaged chain length of odd carbon numbered *n*-alkanes from carbon number 27 to 33.

[b] CPI_{27-33}: carbon preference index of *n*-alkanes from carbon number 27 to 33.

[c] Norm31 = C31/(C31+C29)

[d] Norm33 = C33/(C33+C29)

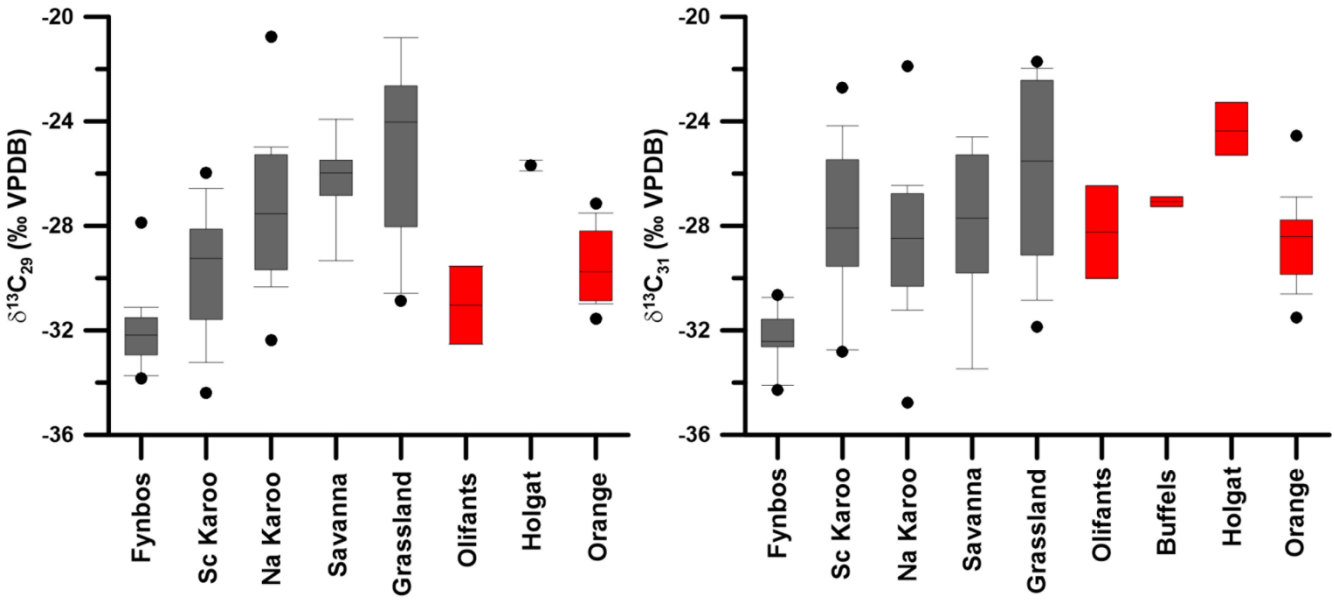

Figure 3: Box and whisker plots for the compound-specific carbon isotopes of the C_{29} (left) and C_{31} (right) *n*-alkanes divided into biome/soil and river samples. Boxes comprise middle 50% of samples and the horizontal black line within the box represents the median. Black dots outside the whisker plots indicate the uppermost and lowermost 10%. Note, for the Holgat River only one $\delta^{13}C_{29}$ data point is available and the horizontal black line indicates the standard deviation of this data point. Na Karoo and Sc Karoo indicate Nama Karoo and Succulent Karoo, respectively.

4.2.2 River-derived samples

Long-chain *n*-alkane concentrations (sum of C_{25}-C_{33}) of the suspension loads vary between 4 and 23 µg/g sediment and show a strong odd-over-even carbon number predominance with $CPI_{27\text{-}33}$ values ranging between 4.1 and 8.4 (Table 3). The $ACL_{27\text{-}33}$ values of the suspension loads vary between 29.8 and 31.0 and the Norm31 and Norm33 ratios range from 0.56 to 0.87 and 0.35 to 0.71, respectively (Table 3). $\delta^{13}C$ values range from -30.9‰ to -27.2‰ (C_{29}) and -29.9‰ to -24.5‰ (C_{31}), respectively.

Long-chain *n*-alkane concentrations of flood deposits show broader variations from 1 to 153 µg/g sediment (Table 3). $CPI_{27\text{-}33}$ values are high for all flood deposits and

range between 3.0 and 24.3 and ACL_{27-33} values vary from 29.8 to 31.5 (Table 3). The Buffels and Holgat River show similar *n*-alkane distributions with a distinctly high relative abundance of the C_{31} alkane (Fig. 2). The Olifants and Orange rivers also show a dominance of the C_{31} alkane but a more evenly distributed *n*-alkane pattern. The Norm31 and Norm33 ratios show a broad range across the flood deposit samples spanning 0.54 to 0.94 and 0.31 to 0.89, respectively (Fig. 2, Table 3). $\delta^{13}C$ range from -32.5‰ to -25.7‰ (C_{29}) and -31.5‰ to -23.3‰ (C_{31}), respectively (Fig. 3).

The Orange River shows increasing compound-specific $\delta^{13}C$ downstream from the Vaal-Orange confluence in both suspension loads and in the flood deposits. Generally, suspension loads have more positive $\delta^{13}C_{31}$ than the flood deposits (Fig. 4). Flood deposits from the west coast rivers show increasing $\delta^{13}C$ from south to north (Table 3).

Table 3: *n*-Alkane abundance, distribution parameters and compound-specific $\delta^{13}C$ compositions of the river samples. Suspension samples are shaded in grey.

No.	Sample name	Sample type	River system	Latitude (°S)	Longitude (°E)	*n*-alkane content$_{25-33}$ (µg/g sed)	ACL_{27-33}[a]	CPI_{27-33}[b]	Norm31[c]	Norm33[d]	$\delta^{13}C_{29}$ (‰ VPDB)	$\delta^{13}C_{31}$ (‰ VPDB)
O1	ORF 8	flood dep.	Olifants	31°36.420	18°24.256	3.2	29.9	9.4	0.55	0.31	-32.5 ± 0.1	-30.0 ± 0.1
O2	ORF 10S	suspension	Olifants	31°33.908	18°19.657	12	31.0	5.7	0.79	0.67	-29.5 ± 0.1	-26.5 ± 0.1
O3	ORF 14	flood dep.	Buffels	29°59.520	17°52.481	150	31.5	21.9	0.94	0.89	n.d.	-26.9 ± 0.2
O4	ORF 15	flood dep.	Buffels	29°34.983	17°15.276	47	31.2	20.0	0.90	0.77	n.d.	-27.3 ± 0.1
O5	ORF 20	flood dep.	Holgat	28°55.960	16°46.497	42	30.9	22.6	0.88	0.54	n.d.	-25.3 ± 0.2
O6	ORF 21	flood dep.	Holgat	28°55.901	16°46.557	65	31.3	19.6	0.92	0.80	n.d.	-24.4 ± 0.5
O7	ORF 22	flood dep.	Holgat	28°55.886	16°46.565	17	31.2	24.3	0.91	0.77	-25.7 ± 0.2	-23.3 ± 0.0
O8	ORF 24S	suspension	Orange	28°33.987	16°30.287	23	31.0	8.4	0.87	0.71	-27.2 ± 0.2	-24.5 ± 0.1
O9	ORF 23	flood dep.	Orange	28°32.006	16°36.509	7.3	30.9	12.2	0.80	0.63	n.d.	-26.9 ± 0.0
O10	ORF 25	flood dep.	Orange	28°05.569	16°52.921	1.1	30.9	10.9	0.80	0.62	n.d.	-27.9 ± 0.1
O11	ORF 26	flood dep.	Orange/Fish	28°05.586	17°10.540	3.8	31.1	12.1	0.81	0.69	-28.2 ± 0.0	-27.6 ± 0.0
O12	ORF 27S	suspension	Orange	28°46.224	17°38.408	17	30.3	3.0	0.69	0.49	-29.4 ± 0.1	-27.8 ± 0.3
O13	ORF 29T	flood dep.	Orange	28°44.458	19°19.970	6.1	29.8	8.5	0.54	0.32	-31.6 ± 0.0	-28.9 ± 0.2
O13	ORF 29B	flood dep.	Orange	28°44.458	19°19.970	1.2	30.6	9.8	0.68	0.52	n.d.	-28.0 ± 0.1
O13	ORF 29S	suspension	Orange	28°44.458	19°19.970	19	29.8	4.1	0.56	0.37	-30.6 ± 0.1	-28.4 ± 0.1
O14	ORF 33	flood dep.	Orange	28°38.182	21°05.437	0.7	30.8	10.4	0.75	0.62	-29.4 ± 0.3	-30.0 ± 0.1
O15	ORF 31S	suspension	Orange	28°38,152	21°05.393	16	30.0	7.5	0.62	0.35	-30.9 ± 0.4	-29.4 ± 0.2
O16	ORF 40	flood dep.	Orange	29°04.296	23°38.232	6.4	31.2	10.2	0.76	0.71	-31.0 ± 0.3	-31.5 ± 0.1
O17	ORF 37	flood dep.	Orange	29°09.652	23°41.816	1.0	30.4	7.8	0.66	0.56	-27.5 ± 0.0	-27.8 ± 0.1
O17	ORF 36S	suspension	Orange	29°09.669	23°41.817	4.8	30.6	5.2	0.69	0.55	-30.5 ± 0.1	-29.8 ± 0.3
O18	ORF 35	flood dep.	Vaal	29°04.202	23°44.439	3.5	31.0	11.7	0.84	0.69	n.d.	-30.6 ± 0.1
O18	ORF 34S	suspension	Vaal	29°04.167	23°44.448	4.0	30.7	8.1	0.69	0.55	-29.8 ± 0.3	-29.9 ± 0.2

n.d. = not determined

[a] ACL_{27-33}: averaged chain length of odd carbon numbered *n*-alkanes from carbon number 27 to 33.

[b] CPI_{27-33}: carbon preference index of *n*-alkanes from carbon number 27 to 33.

[c] Norm31 = C31/(C31+C29)

[d] Norm33 = C33/(C33+C29)

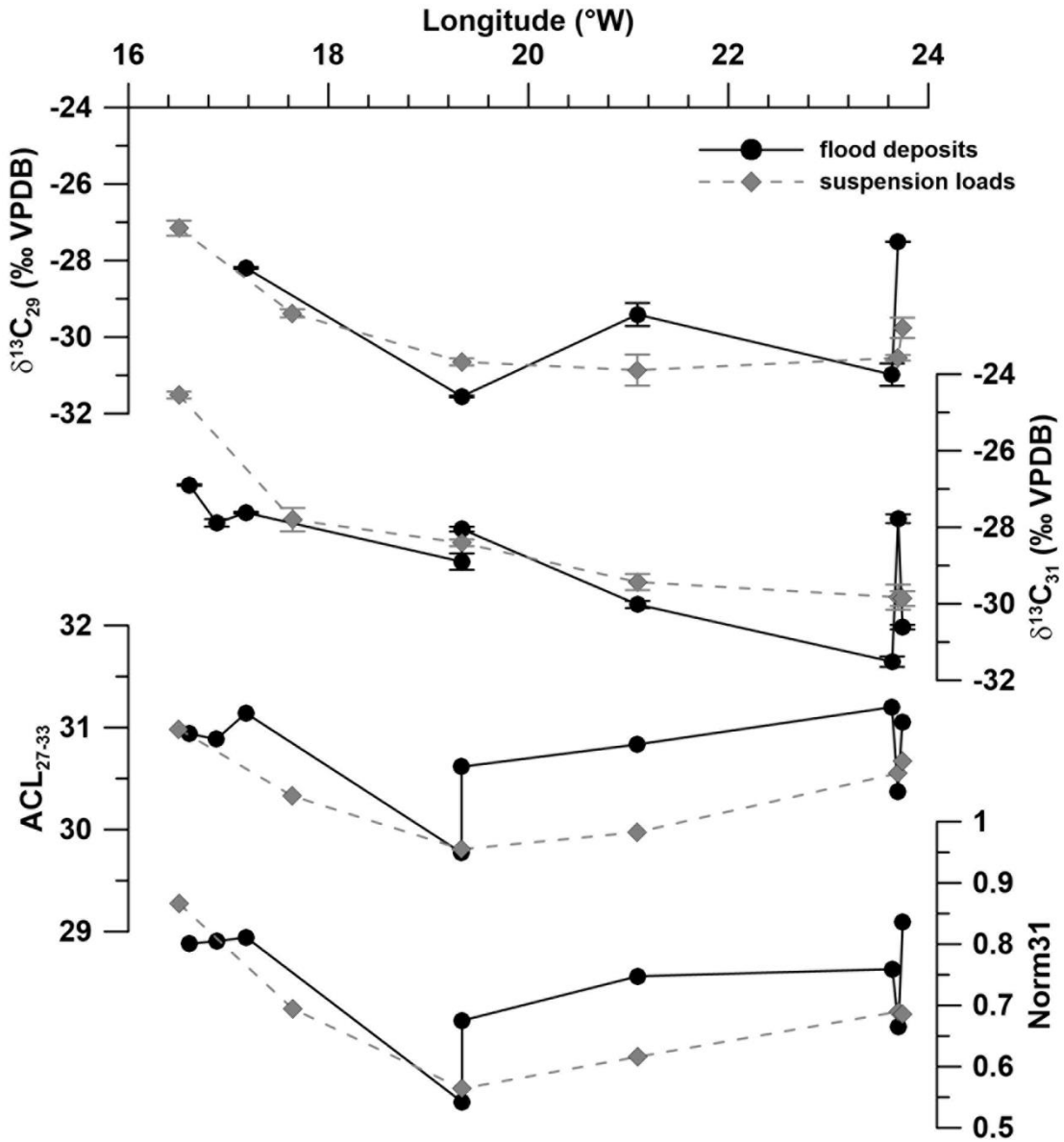

Figure: 4: Compound-specific carbon isotopes of *n*-alkanes C_{29} and C_{31}, ACL_{27-33} and Norm31 for flood deposits (black dots) and suspension loads (grey diamonds) along the transect from the Vaal-Orange confluence (right) to the Orange River mouth (left).

4.2.3 Marine surface sediments

Long-chain *n*-alkanes were found in all surface sediment samples and concentrations (sum of C_{25}-C_{33}) range between 2 and 31 µg/g sediment (Table 4). In general, lowest *n*-alkane concentrations occur in the northern (locations 1 and 2) and southern (locations 5 - 9) parts of the mudbelt. CPI_{27-33} values for all surface sediments range from 9.1 to 14.7

and the ACL_{27-33} varies only slightly between 30.8 and 31.2 (Table 4). In all surface sediments the *n*-alkane distribution is dominated by the C_{31} alkane (Fig. 2, Fig. 5). The Norm31 and Norm33 ratios cover a range spanning from 0.78 to 0.84 (Fig. 6) and 0.60 to 0.72, respectively (Table 4).

Table 4: *n*-Alkane abundance, distribution parameters and compound-specific $\delta^{13}C$ compositions of the marine surface samples.

No.	Core site	Depth (cm)	Water depth (m)	Latitude (°S)	Longitude (°E)	*n*-alkane content$_{25-33}$ (µg/g sed)	ACL_{27-33}[a]	CPI_{27-33}[b]	Norm31[c]	Norm33[d]	$\delta^{13}C_{29}$ (‰ VPDB)	$\delta^{13}C_{31}$ (‰ VPDB)
1	8332-3	0-1	117	29°07.66	16°39.56	3.2	30.8	9.5	0.78	0.60	-28.0 ± 0.1	-26.7 ± 0.1
2	8331-2	0-1	88	29°08.13	16°42.86	3.7	31.0	9.1	0.80	0.64	-28.8 ± 0.1	-27.0 ± 0.2
3	8327-1	0-1	88	29°42.19	17°00.42	8.3	31.2	11.8	0.83	0.70	-27.5 ± 0.1	-26.0 ± 0.1
4	8325-1	0-1	134	30°35.70	17°16.73	31	31.2	14.7	0.84	0.72	-27.4 ± 0.1	-26.0 ± 0.0
5	8324-1	0-1	100	31°44.83	18°05.47	6.4	31.2	14.2	0.83	0.70	-27.5 ± 0.2	-26.0 ± 0.1
6	8321-1	0-1	104	31°51.81	18°07.01	6.1	31.1	12.9	0.81	0.67	-27.6 ± 0.2	-25.9 ± 0.0
7	8322-1	0-1	105	31°57.22	18°07.07	5.5	31.1	12.0	0.79	0.65	-27.9 ± 0.0	-26.0 ± 0.0
8	8323-1	0-1	90	32°01.89	18°13.29	6.0	31.1	13.7	0.82	0.67	-28.5 ± 0.0	-26.3 ± 0.0
9	8319-1	0-1	69	32°29.74	18°04.70	2.4	31.0	11.9	0.78	0.64	-28.4 ± 0.3	-26.5 ± 0.1

[a] ACL_{27-33}: averaged chain length of odd carbon numbered *n*-alkanes from carbon number 27 to 33.
[b] CPI_{27-33}: carbon preference index of *n*-alkanes from carbon number 27 to 33.
[c] Norm31 = C31/(C31+C29)
[d] Norm33 = C33/(C33+C29)

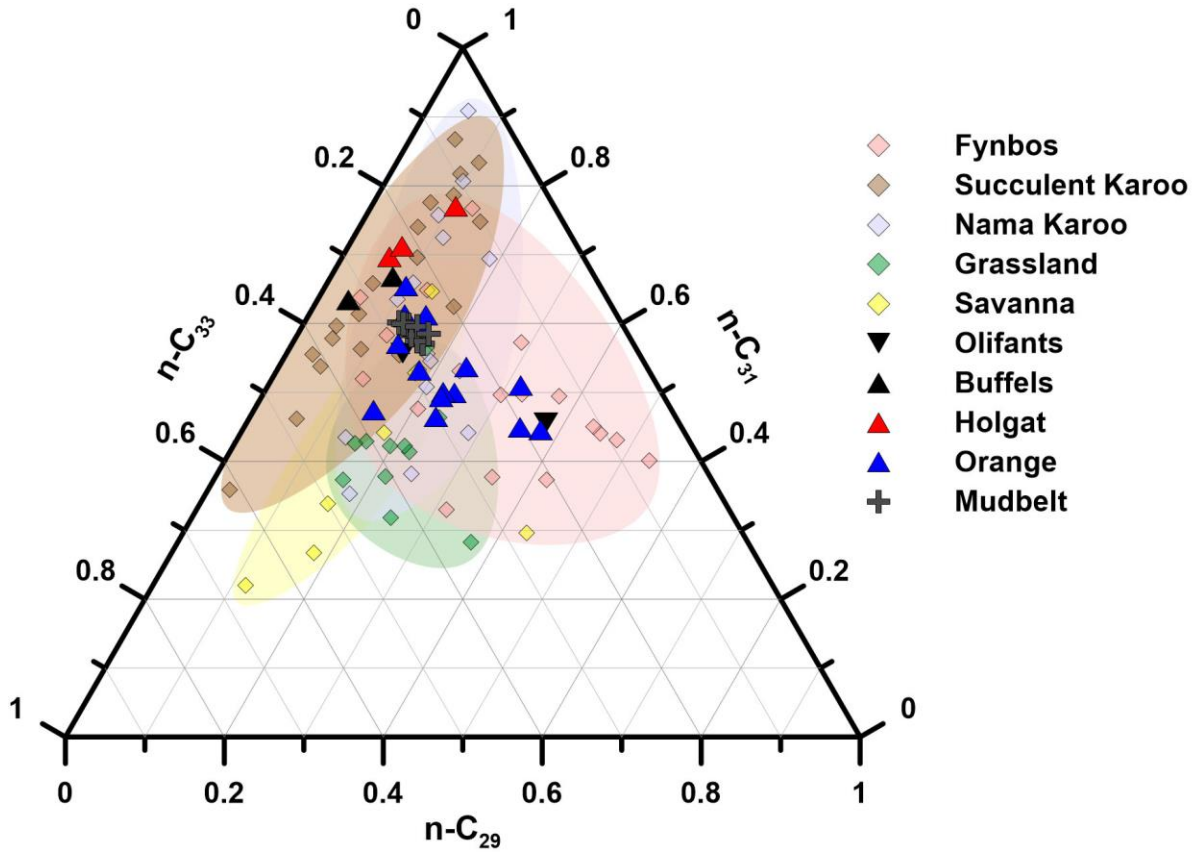

Figure 5: The relative abundances of the *n*-alkanes C_{29}, C_{31} and C_{33} by different sample groups. Diamonds represent soils from the different biomes, triangles represent flood deposits and suspension loads of the different river systems and crosses represent marine surface sediments. Coloured areas indicate the range of different biomes, the outlier for the savanna soils is excluded.

$\delta^{13}C$ values of the C_{29} (Fig. 6) and the C_{31} alkanes range from -28.8‰ to -27.4‰ and -27.0‰ to -25.9‰, respectively (Table 4). Most depleted values are observed in the northern mudbelt, with increasing values towards the central mudbelt and decreasing again in the southern mudbelt (Fig. 6).

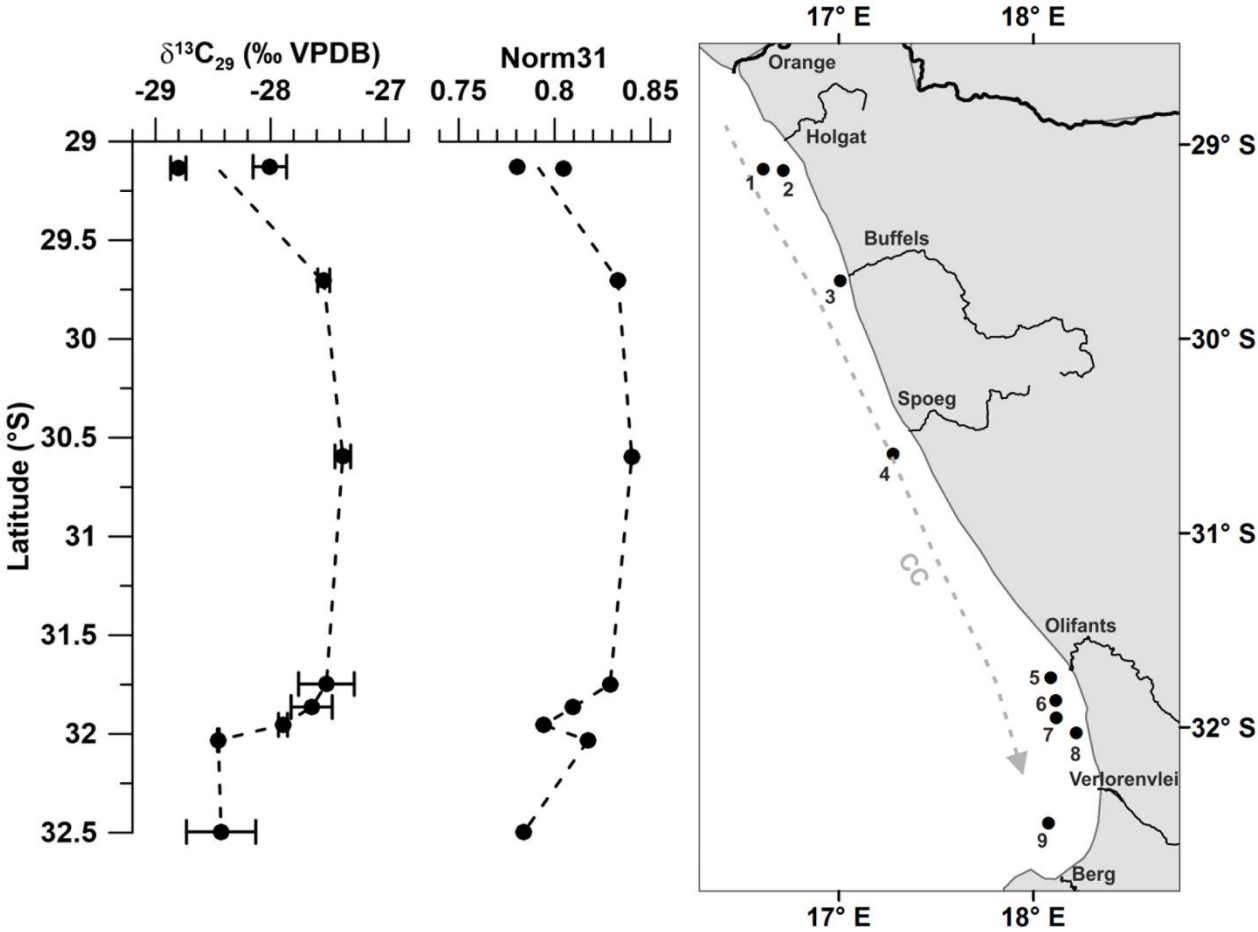

Figure 6: Compound-specific stable carbon isotope composition of C_{29} (left) and Norm31 (right) for surface sediments along the west coast of South Africa. Position of the poleward countercurrent (CC) is indicated by the grey dotted line.

5 Discussion

To determine the palaeoenvironmental significance of plant biomarkers preserved within southwestern African mudbelt sediments it is crucial to first characterize the source signals in the various catchment areas and their potential alteration during riverine transport.

5.1 Characterization of source signals reflected in soils of the different biomes

The predominance of long-chain *n*-alkanes and the CPI values higher than 4 of most *n*-alkanes in soils indicate an origin from terrestrial higher plants and a relatively non-degraded state (Eglinton and Hamilton, 1967). Similarly high CPI values are reported for soils in other regions, including semi-arid to humid climates (e.g. Bush and McInerney, 2015; Kuhn et al., 2010; Schwab et al., 2015). In particular, succulent plants, such as Aizoaceae or Crassulaceae, tend to produce higher amounts of plant waxes than, for instance, grasses which is also found to be reflected in corresponding soils (Carr et al., 2014; Garcin et al., 2014). The *n*-alkane concentrations in soils of the different biomes from this study are consistent with these previously observed trends (Table 2) which can likely be attributed to differential production of plant waxes by the distinct plant types.

Soils in the Succulent Karoo and Nama Karoo biomes show comparable *n*-alkane distributions to modern plants from these biomes (Boom et al., 2014; Carr et al., 2014). They show a tendency towards longer chain lengths and greater proportions of the C_{33} *n*-alkane (Fig. 2). Additionally, the different *n*-alkane distribution patterns (Norm31 and Norm33 ratios) reflect the distinct plant communities in the different biomes. For instance, C_4 grasses are known to generally produce C_{31} and C_{33} *n*-alkanes in higher abundance than C_3 trees and C_3 grasses (Bush and McInerney, 2013; Rommerskirchen et al., 2006b; Vogts et al., 2009). Bush and McInerney (2015), however, inferred that growing season temperature rather than the photosynthetic pathway is the main driver of chain length distribution. The typical *n*-alkane distribution pattern for C_4 grasses with a dominance of C_{31} and C_{33} is particularly reflected in soils of the Grassland Biome (Fig. 2). This biome also exhibits the most enriched average ^{13}C values (Table 2). Nevertheless, the range of compound-specific $\delta^{13}C$ for the Grassland Biome is large (Fig. 3) and it has to be taken into account that the Grassland Biome does not only

consists of C_4 grasses, but also of C_3 plants (~ 40% coverage), including trees, shrubs and grasses (Cowling et al., 1999; Werger and Ellis, 1981). Therefore, soils in the Grassland Biome can show on average a mixture of photosynthetic pathways. The compound-specific $\delta^{13}C$ composition of Succulent Karoo and Nama Karoo soils is more ^{13}C-depleted than the Grassland or Savanna soils, reflecting not only the occurrence of more C_3 plants in the Succulent Karoo. However the values are still higher than those observed in a C_3 biome (e.g. Fynbos) reflecting the abundance of drought-tolerant succulent CAM plants (Boom et al., 2014; Cowling et al., 1999; Feakins and Sessions, 2010; Mooney et al., 1977; Werger and Ellis, 1981). A higher abundance of the C_{29} *n*-alkane and more depleted $\delta^{13}C$ values distinguish the soils in the Fynbos Biome from the other biomes (Fig. 2, Fig. 3). Although, the geochemical proxies in soils from the other biomes (Succulent Karoo, Nama Karoo, Grassland and Savanna) differ on average, they are not clearly distinguishable from each other due to the large internal variability.

5.2 The overprinting of river-transported signals by local vegetation

5.2.1 Olifants River:

The comparison of the flood deposit (O1, Fig. 1) and the contemporary suspension load (O2, Fig. 1) of the Olifants River reveals differing *n*-alkane distributions and compound-specific $\delta^{13}C$ values, despite both sampling sites being located in the Succulent Karoo. The plant wax-derived signals of the suspension load, sampled in the dry season, exhibit similarities with Succulent Karoo soils and plants (Carr et al., 2014). For instance, ACL_{27-33} (31.0) and $\delta^{13}C$ composition of C_{29} (-29.5‰) and C_{31} (-26.5‰) lie in the range of Succulent Karoo soils (31.2 ± 0.4, -29.8 ± 2.4‰, -27.9 ± 2.8‰) rather than Fynbos soils (30.5 ± 0.6, -32.1 ± 1.4‰, -32.3 ± 1.0‰), implying local input during the dry season

(Table 2, Table 3). By contrast the flood deposit, with lower ACL, Norm31, Norm33 and compound-specific $\delta^{13}C$ than the suspension load (Table 3), is more comparable to plants (Carr et al., 2014) and soils in the Fynbos Biome (Table 2) and likely reflects greater input from this C_3 dominated biome, located upstream in the Olifants catchment. Based on this observation, we surmise that flood-events sourced in the Cederberg Mountains of the Fynbos Biome may produce an identifiable signature, whereas during non-flood conditions and/or dry season the source area of the terrestrial material may lie closer to the coastal sampling location of the suspension load. However, we cannot rule out that the flood deposit may be either much older than the suspension load, reflecting a different climate/vegetation regime, and/or that the flood was characteristic of such events. Heavy rains are more common in the mountains, but large storms may also cause extensive flooding in the Succulent Karroo, and it is likely that sediments transported by these different events will show different geochemical signatures. Hence, this finding does not allow us to estimate modern Fynbos Biome contributions during the rainy season.

5.2.2 Ephemeral west coast rivers:

The Buffels and the Holgat River only drain the Succulent Karoo Biome (Fig. 1). The flood deposits of both rivers (O3-O7, Fig. 1) were sampled from the riverbeds, and are likely relatively recent as these rivers experience regular (every 5–10 years) floodings (Benito et al., 2011a). They show the highest ACL and Norm ratios in this study and compare well to Succulent Karoo soils (Table 2) and plants (Carr et al., 2014). Furthermore, the $\delta^{13}C_{31}$ of the flood deposits from the Buffels River (-27.1 ± 0.2‰) are in the range of $\delta^{13}C_{31}$ of the Succulent Karoo soils (-27.9 ± 2.8‰, Table 2) and therefore likely reflect the modern Succulent Karoo vegetation. In contrast, the $\delta^{13}C_{31}$ for the

Holgat River flood deposits are higher (-24.8 ± 0.8‰) than the Succulent Karoo. CAM plants are known to have very variable $\delta^{13}C$ compositions often lying between C_3 and C_4 plants, but also reaching values as high as -14‰ (e.g. Boom et al., 2014; Chikaraishi and Naraoka, 2003).. The catchment of the Holgat River is drier than the Buffels River (Bickerton, 1981a; Cowling et al., 1999; Heinecken, 1981), which may foster a distinct vegetation cover and/or differing usage of CAM photosynthesis (Born et al., 2006; Desmet, 1996) leading to differences in their $\delta^{13}C$ composition. Further, the modern suspension load closest to the Orange River mouth (Fig. 4) has a similar $\delta^{13}C$ composition (-24.5 ± 0.1‰) to the Holgat River flood deposits (Fig. 3) possibly indicating a specific vegetation signal from this area (Born et al., 2006). As before, it is also possible that differences in the *n*-alkane $\delta^{13}C$ of the Holgat and Buffels rivers results from different ages of the flood deposits. Overall, the Holgat River catchment seemingly contains a more specialised vegetation adapted to drier conditions than the Buffels River catchment (Bickerton, 1981a; Born et al., 2006; Heinecken, 1981; Mucina and Rutherford, 2006) likely leading to a more enriched $\delta^{13}C$ composition in Holgat than Buffels River flood deposits and Succulent Karoo soils.

5.2.3 Orange River:

An important observation is that the *n*-alkane distribution patterns of the suspension loads (Fig. 4) change downstream as the Orange River flows through different biomes (Fig. 1). In general, compound-specific $\delta^{13}C$ increases downstream (Fig. 4). This implies an overprint of the transported signal by contributions from local vegetation sources along the river course from the drier Nama and Succulent Karoo biomes.. This overprint results in a similarity in *n*-alkane parameters between the suspension load closest to the Orange River mouth (O8, Fig. 4) and those in the flood deposits of the Holgat River (O5-

O7, Fig. 2). Gray (2009) also interpreted the $\delta^{13}C$ of bulk TOC in modern sediments from the bedload of the lower Orange River to reflect organic matter contributions from surrounding areas and river bank vegetation. Inorganic geochemical data ($^{87}Sr/^{86}Sr$ and εNd) of the samples analysed for this study support this finding, implying sediment contributions from along the Orange River (Hahn et al., 2015). This contrasts with earlier studies that inferred that terrestrial material transported by the Orange River is primarily sourced in the Drakensberg Mountains from Karoo sedimentary rocks (Compton and Maake, 2007; de Villiers, 2000; Mabote et al., 1997).

A comparison of organic and inorganic geochemical proxies for the suspension loads upstream near the Orange-Vaal confluence, however, reveals a more complex picture. While the *n*-alkane compositions of suspension loads from the Vaal (O18) and Orange Rivers immediately upstream of the confluence (O17) are similar at this location (Fig. 4, Table 3), the inorganic components indicate a variety of sedimentary sources (Hahn et al., 2015). These findings imply, to a certain extent, a decoupling of source areas for organic and inorganic material transported by the Orange River. The inorganic material might comprise a more hinterland signal probably due to higher weathering rates in its source region than in the lower river course (Compton and Maake, 2007; de Villiers, 2000; Le Roux, 1990; Mabote et al., 1997). In contrast, a continuous contribution of the adjacent vegetation along the river course might overprint the organic matter signal. A similar de-coupling of organic and inorganic sedimentary signals has also been inferred for other major river systems, e.g. the Zambezi River (Just et al., 2014; Schefuß et al., 2011).

The *n*-alkane distribution patterns and compound-specific $\delta^{13}C$ for flood deposits show similar trends as the suspension loads downstream the Orange River (Fig. 4).

However, unlike the suspension samples, the flood deposits upstream of the confluence with the Vaal River (Fig. 1) differ in their *n*-alkane distributions and $\delta^{13}C$ compositions. The Orange River flood deposit (O17) shows lower ACL_{27-33}, Norm31 and Norm33 ratios as well as higher $\delta^{13}C$ values than the Vaal flood deposit (O18, Fig. 4, Table 3). The difference between flood deposits and suspension loads at the Orange-Vaal confluence may therefore indicate different sources for flood deposits and suspension loads within the Orange River system. For instance, soils of the Grassland Biome have on average higher $\delta^{13}C$ values for C_{29} and C_{31} than those of the Savanna and Nama Karoo biomes (Fig. 3, Table 2). The ACL_{27-33} and Norm31 ratio are also lower for Grassland soils compared to Savanna and Nama Karoo soils (Fig. 2, Table 2). Thus, the flood deposit of the Orange River upstream of the confluence could have originated in the more humid eastern Nama-Karoo transition zone to the Grassland Biome. It is important to consider that flood events integrate larger, albeit perhaps heterogeneous, spatial extents, and while occurring at a discrete point in time, they may entrain much older material as they erode the landscape. Comparison between flood deposits and suspension loads is thus problematic, particularly as our suspension load samples were collected only once and solely reflect a snapshot of the total fluvially-transported material. Another complicating factor is the age of the flood deposits. The Orange River flood deposit (O17) is older (856 ± 65 cal. years BP) than the Vaal River flood deposit (515 ± 20 cal. years BP) (Table 1), and differences in *n*-alkane compositions for both the flood samples and the suspension load samples may be a result of changes in climate and vegetation through time (Chevalier and Chase, 2015; Holmgren et al., 2003; Scott et al., 2012). Additionally, modern commercial farming and grazing, accounting for ~ 80% of the total land area of South Africa (DAFF, 2016), has also possibly biased the signal in the modern

suspension loads. At present, we have no conclusive argument whether it was a change in sediment source or climate/vegetation that was the dominant factor determining the observed variability, but nevertheless the increasing compound-specific $\delta^{13}C$ trend downstream the Orange River is similar for both sample types.

In general, this study indicates that terrestrial organic material discharged by the Orange River represents a heterogeneously integrated catchment signal, whereas all of the west coast rivers exhibit biomarker signals consistent with their locations in different vegetation zones. Flood deposits indicate that such events can carry a signal from the hinterland, while under non-flood conditions the suspension load more reflects the local vegetation. To evaluate whether flood events, especially in the ephemeral Succulent Karoo rivers, or the non-flood conditions stronger contribute more or less significantly to the mudbelt sediments, further investigations are needed.

5.3 Sources of terrestrial organic matter in the southwest African mudbelt

In marine surface sediments CPI values higher than 7 imply minor degradation of the long-chain *n*-alkanes and an origin from terrestrial higher plants (Eglinton and Hamilton, 1967). The ternary diagram (Fig. 5) of relative C_{29}, C_{31} and C_{33} *n*-alkane abundance indicates that the *n*-alkane distributions of the marine surface sediments plot in the overlapping area of all biomes. This finding suggests a mixed signal derived from different source areas in the catchments of the Orange River and the west coast rivers. In all mudbelt samples the C_{31} *n*-alkane is more abundant than the C_{29} and C_{33} *n*-alkanes and overall there is low variability in *n*-alkane distribution across the mudbelt (Fig. 2). Mudbelt surface sediment $\delta^{13}C_{31}$ compositions (-25.9‰ to -27.0‰) are more enriched but show a range and trend similar to $\delta^{13}C_{29}$ (-27.4‰ to -28.8‰). While the C_{31} *n*-alkane is dominant in all biomes (Fig. 2), it tends to be produced in higher amounts by

succulent plants (Carr et al., 2014) and grasses (Vogts et al., 2009), the latter being present in all biomes. Given this observation, despite the higher abundance of the C_{31} *n*-alkane in the marine surface sediments, the $\delta^{13}C$ of C_{29} is likely more informative about vegetation sources and is used here to discuss changes in terrestrial organic input. Although the *n*-alkane parameters do not show large amplitude changes for the marine surface sediments (Fig. 6) compared to the soils, clear trends are evident along the transect, which likely are caused by sedimentary input from differential sources.

The northernmost mudbelt sediments, closest to the Orange River and located near the Holgat River mouth (locations 1–2, Fig. 1, Fig. 6), show $ACL_{27\text{-}33}$ values lower or equal to 31.0 and Norm31 and Norm33 ratios below or equal to 0.80 and 0.64, respectively (Table 4). These values lie in the range of the biomes drained by the Orange River and its suspension loads (Fig. 2, Fig. 4). Compound-specific $\delta^{13}C$ compositions of the surface sediments (-28.0‰ to -28.8‰) also lie within the range of the biomes (-25.2‰ to -29.8‰) drained by the Orange River and the Orange River suspension loads (-27.3‰ to -30.9‰). In contrast, Holgat River flood deposits reach higher $ACL_{27\text{-}33}$ (31.1 ± 0.2), Norm31 (0.90 ± 0.02), Norm33 (0.70 ± 0.12) as well as more enriched $\delta^{13}C$ (-25.7 ± 0.2‰) compositions (Fig. 2, Table 2). This implies that terrestrial organic matter in the northernmost mudbelt is largely derived from the Orange River and likely reflects a variably integrated signal of biomes drained by the Orange River. Zhao et al. (2015) investigated the pollen distribution in the same mudbelt surface sediments and found increased percentages of Poaceae (a dominant component of the Nama-Karoo, Grassland and Savanna biomes) and pollen from riparian taxa (Cyperaceae, *Phragmites*-type and *Typha*) in the northern mudbelt sediments, also implying a dominant source in the Orange River catchment.

Further south in the central mudbelt (locations 3-4, Fig. 6), the *n*-alkane proxies indicate an additional contribution from the CAM-rich Succulent Karoo Biome. This input manifests itself in increased ACL_{27-33} (31.2), Norm31 (0.83 to 0.84), Norm33 (0.70 to 0.72) and slightly higher $\delta^{13}C$ (-27.5 ‰ to -27.4‰) (Fig. 6, Table 4). Similar signals are detected for the flood deposits of the ephemeral Holgat and Buffels rivers (Fig. 2, Fig. 3) with higher ACL_{27-33} (31.1 to 31.4), Norm31 (0.90 to 0.92) and Norm33 (0.70 to 0.83) compared to the Orange River suspension loads and flood deposits. In terms of relative contributions from the various catchments, although the southward countercurrent transports Orange River derived sediments to the south, Mabote et al. (1997) argued that the countercurrent is not strong enough to transport medium to fine silt sediments as far south as the Buffels River mouth. In addition, increasing *n*-alkane concentrations from the northern to the central mudbelt (Table 4) indicate additional input from the adjacent continent. This is consistent with higher *n*-alkane concentrations in Succulent Karoo soils and in the flood deposits of the Holgat and Buffels rivers compared to other biomes and rivers (Table 2). Further, the C_{29} *n*-alkane in the Holgat River flood deposit (O7) is more ^{13}C-enriched (-25.7 ± 0.2‰) than the Orange River suspension loads and flood deposits (-27.8 ± 0.6‰) (Fig. 4, Table 3). Pollen analyses show a slight increase of Aizoaceae and Asteraceae pollen abundances relative to grasses and riparian taxa in the central mudbelt sediments, likely reflecting higher contributions from the adjacent Nama Karoo and Succulent Karoo vegetation (Gray et al., 2000; Zhao et al., 2015). Nevertheless, the increased importance of Aizoaceae pollen in the central mudbelt sediments is less pronounced than the increase of compound-specific $\delta^{13}C$ values, which is not very surprising as Aizoaceae tends to produce relatively high amounts of plant waxes (Carr et al., 2014) but only low amounts of pollen (Dupont and Wyputta,

2003). Additionally, Mabote et al. (1997) detected diverging grain-size trends in cores off the Orange and the Buffels River pointing to an additional sedimentary input by the Buffels River. It thus seems plausible that the terrestrial organic signals derived from the Orange River are overprinted by terrigenous contributions from the Holgat and Buffels rivers. However, despite the indications for a higher Succulent Karoo influence, we cannot differentiate terrestrial input from aeolian versus fluvial transport. Nevertheless, as the west coast wind regimes are dominantly southerly (Tyson and Preston-Whyte, 2000) it is likely that both aeolian and fluvial transport are dominated by material sourced from the western coastal margin.

In the southern mudbelt (locations 5-9) the shift to lower $\delta^{13}C_{29}$, ACL and Norm ratios (Fig. 6) can be attributed to the proximity of the Fynbos Biome, where soils are more depleted in *n*-alkane ^{13}C (Fig. 3) and have lower ACL and Norm ratios (Fig. 2) than the Succulent Karoo soils (Table 4) (Carr et al., 2014). This is consistent with the higher occurrence of Restionaceae pollen (primarily restricted to the Fynbos Biome) in the southern mudbelt sediments (Zhao et al., 2015) as well as with findings of significant contributions from Olifants River suspension loads (Hahn et al., 2015).

An interesting finding of this work is that the northernmost mudbelt surface sediments show comparable *n*-alkane parameters and compound-specific $\delta^{13}C$ as the southernmost mudbelt surface sediments. Based on the pollen data (Zhao et al., 2015), and considering that the Orange River today is the by far greatest supplier of sediment to the northern mudbelt (Birch et al., 1991; Bremner et al., 1990), it is, however, unlikely that the biomarker signal in the northern mudbelt is derived from the Fynbos Biome. It can, therefore, reasonably assumed that the observed trends in terrestrial organic signals in mudbelt sediments reflect local inputs and not long-range transported signals.

In order to estimate the magnitude of *n*-alkane input by the Orange River and the west coast rivers along the north-south transect in the mudbelt, we applied a binary mixing model using compound-specific $\delta^{13}C$. We assume that a change in the northern and central mudbelt is attributed to an additional input of *n*-alkanes derived from the west coast rivers draining the Succulent Karoo and therefore define the two end-members as 1) the arithmetic mean of the weighted mean $\delta^{13}C$ (C_{29} and C_{31}) for the suspension loads of the Orange River (-28.7 ± 2.0‰) and 2) the mean for the flood deposits of the Buffels and Holgat rivers (-25.5 ± 1.6‰). This leads to an increasing *n*-alkane contribution of about 33 ± 13% (from 30 – 57% to 64 – 90%) by the smaller west coast rivers from the northern to the central mudbelt. Towards the southern mudbelt, we proceed with the assumption that a change in $\delta^{13}C$ in the southern mudbelt sediments is attributed to an input of Fynbos derived *n*-alkanes. For the Fynbos end-member we used the weighted mean $\delta^{13}C$ of the suspension load from the Olifants River (-31.2 ± 1.3‰), which is suggested to reflect the Fynbos signal. Based on this, the Fynbos signal increases by 12 ± 11% from the Olifants River mouth (4 – 25%) to the southernmost location 30km north of the Berg River mouth (16 – 37%). We note, however, that these estimates are based on several assumptions and absolute numbers should be taken with caution. Additionally, aeolian transport from the coastal west coast biomes might contribute to the leaf wax inventory of the mudbelt. To evaluate the relative contribution of aeolian vs. fluvial transport to the mudbelt, further investigations are needed. Nevertheless, the estimation indicates that the terrestrial organic material in the mudbelt is derived not only from the Orange River, but also from the western coastal margin, including the Succulent Karoo, and, increasingly to the south, the Fynbos Biome. Considering these observations in terms of palaeoenvironmental research, they imply

that a multiproxy approach in conjunction with other terrestrial proxies, such as pollen, allows to differentiate between terrestrial organic sources in the northern and southern mudbelt and more reliable palaeoenvironmental interpretations.

6 Conclusions

This study provides an overview of sources, effects of transport and depositional patterns of terrestrial organic material in the western South Africa coastal mudbelt. Based on terrestrial leaf wax *n*-alkane investigations of soils, river suspension loads and flood deposits, and marine sediments we found that:

i) Biomes within the Orange River and west coast river catchments show on average differences in *n*-alkane distributions and compound-specific $\delta^{13}C$ compositions, which are attributed to their different vegetation types, despite a large variability of individual samples.

ii) Terrestrial organic material transported by the Orange River is overprinted by local downstream vegetation contributions during riverine transport. Therefore, the terrestrial organic material discharged by the Orange River represents a heterogeneously integrated catchment signal.

iii) The influence of the Orange River on the mudbelt sediments declines further south and is overprinted by signals derived from the western coastal margin, including the Succulent Karoo and Fynbos Biome.

Our study underlines the need to identify sources of inorganic and organic terrestrial material for adequate interpretation in environmental reconstructions. Our findings suggest that future studies of mudbelt sediments must consider that 1) Orange River sediments do not necessarily solely reflect changes to the SRZ as a whole, but may

reflect sub-regional dynamics, with a potential bias towards signals from the lower reaches of the river course, and 2) the mudbelt contains sediments from both the Orange river, the central west coast, and the Fynbos Biome, and that the relative contribution of these regions has likely changed significantly over time (Birch et al., 1991). Considering the presented data and regional oceanic and atmospheric circulation patterns, it may be inferred that sediments in the southern mudbelt are likely well-suited to reconstruct palaeoenvironmental changes in the southwestern WRZ. While more complex, we suggest that using a multiproxy approach parallel investigations of northern and southern mudbelt sediments may allow reconstructions of palaeoenvironmental changes in at least some parts of the SRZ and the dynamics between these regions and the WRZ.

7 Acknowledgments

This study was funded by the Bundesministerium für Bildung und Forschung (BMBF) within the project „Regional Archives for Integrated Investigation" (RAiN, 03G0840A). This work was also supported by the Leverhulme Trust (Grant F/00 212/AF) and the European Research Council (ERC) Starting Grant ''HYRAX'' (Grant Agreement No. 258657). We thank the captain, the crew and the scientists of Meteor cruise M57-1 for recovering the marine sediment samples. Xueqin Zhao and Lydie Dupont are thanked for helpful discussion and Thilo Eickhorst is thanked for help with soil import. We are grateful to Ralph Kreutz and Oliver Helten for analytical assistance. Finally, we thank the two anonymous reviewers for their constructive comments.

8 References

Aichner, B., Herzschuh, U., Wilkes, H., 2010. Influence of aquatic macrophytes on the stable carbon isotopic signatures of sedimentary organic matter in lakes on the Tibetan Plateau. Org. Geochem. 41, 706–718. doi:10.1016/j.orggeochem.2010.02.002

Benito, G., Botero, B.A., Thorndycraft, V.R., Rico, M., Sánchez-Moya, Y., Sopeña, A., Machado, M.J., Dahan, O., 2011a. Rainfall-runoff modelling and palaeoflood hydrology applied to reconstruct centennial scale records of flooding and aquifer recharge in ungauged ephemeral rivers. Hydrol. Earth Syst. Sci. 15, 1185–1196. doi:10.5194/hess-15-1185-2011

Benito, G., Thorndycraft, V.R., Rico, M.T., Sánchez-Moya, Y., Sopeña, A., Botero, B. a., Machado, M.J., Davis, M., Pérez-González, A., 2011b. Hydrological response of a dryland ephemeral river to southern African climatic variability during the last millennium. Quat. Res. 75, 471–482. doi:10.1016/j.yqres.2011.01.004

Bentley, S.J., Blum, M.D., Maloney, J., Pond, L., Paulsell, R., 2016. The Mississippi River source-to-sink system: Perspectives on tectonic, climatic, and anthropogenic influences, Miocene to Anthropocene. Earth-Science Rev. 153, 139–174. doi:10.1016/j.earscirev.2015.11.001

Bi, X., Sheng, G., Liu, X., Li, C., Fu, J., 2005. Molecular and carbon and hydrogen isotopic composition of n-alkanes in plant leaf waxes. Org. Geochem. 36, 1405–1417. doi:10.1016/j.orggeochem.2005.06.001

Bickerton, I.B., 1981a. Holgat (CW2), in: Heydorn, A.E.F., Grindley, T.J.E. (Eds.), Estuaries of the Cape. Part II: Synopses of Available Information on Individual Systems. CSIR Research Report 404, p. 27 pp.

Bickerton, I.B., 1981b. Spoeg (CW5), in: Heydorn, A.E.F., Grindley, T.J.E. (Eds.), Estuaries of the Cape. Part II: Synopses of Available Information on Individual Systems. CSIR Research Report 400, p. 30 pp.

Birch, G.F., 1977. Surficial sediments on the continental margin off the west coast of South Africa. Mar. Geol. 23, 305–337. doi:10.1016/0025-3227(77)90037-8

Birch, G.F., Day, R.W., Du Plessis, A., 1991. Nearshore Quaternary sediments on the west coast of southern Africa. Bull. - Geol. Surv. South Africa 101, 14.

Boom, A., Carr, A.S., Chase, B.M., Grimes, H.L., Meadows, M.E., 2014. Leaf wax n-alkanes and δ13C values of CAM plants from arid southwest Africa. Org. Geochem. 67, 99–102. doi:10.1016/j.orggeochem.2013.12.005

Born, J., Linder, H.P., Desmet, P., 2006. The Greater Cape Floristic Region. J. Biogeogr. 34, 147–162. doi:10.1111/j.1365-2699.2006.01595.x

Bouchez, J., Galy, V., Hilton, R.G., Gaillardet, J., Moreira-Turcq, P., Pérez, M.A., France-Lanord, C., Maurice, L., 2014. Source, transport and fluxes of Amazon River particulate organic carbon: Insights from river sediment depth-profiles. Geochim. Cosmochim. Acta 133, 280–298. doi:10.1016/j.gca.2014.02.032

Bremner, J.M., Rogers, J., Willis, J.P., 1990. Sedimentological aspects of the 1988 Orange River floods. Trans. R. Soc. South Africa 47, 247–294.

Bronk Ramsey, C., 2009. Bayesian Analysis of Radiocarbon Dates. Radiocarbon 51, 337–360. doi:10.2458/azu_js_rc.v51i1.3494

Bush, R.T., McInerney, F.A., 2015. Influence of temperature and C4 abundance on n-alkane chain length distributions across the central USA. Org. Geochem. 79, 65–73. doi:10.1016/j.orggeochem.2014.12.003

Bush, R.T., McInerney, F.A., 2013. Leaf wax n-alkane distributions in and across modern plants: Implications for paleoecology and chemotaxonomy. Geochim. Cosmochim. Acta 117, 161–179. doi:10.1016/j.gca.2013.04.016

Campbell, B.M., Moll, E.J., 1977. The Forest Communities of Table Mountain, South Africa. Vegetatio 34, 105–115.

Carr, A.S., Boom, A., Chase, B.M., Meadows, M.E., Roberts, Z.E., Britton, M.N., Cumming, A.M.J., 2013. Biome-scale characterisation and differentiation of semi-arid and arid zone soil organic matter compositions using pyrolysis–GC/MS analysis. Geoderma 200-201, 189–201. doi:10.1016/j.geoderma.2013.02.012

Carr, A.S., Boom, A., Grimes, H.L., Chase, B.M., Meadows, M.E., Harris, A., 2014. Leaf wax n-alkane distributions in arid zone South African flora: Environmental controls, chemotaxonomy and palaeoecological implications. Org. Geochem. 67, 72–84. doi:10.1016/j.orggeochem.2013.12.004

Chase, B.M., Meadows, M.E., 2007. Late Quaternary dynamics of southern Africa's winter rainfall zone. Earth-Science Rev. 84, 103–138. doi:10.1016/j.earscirev.2007.06.002

Chevalier, M., Chase, B.M., 2015. Southeast African records reveal a coherent shift from high- to low-latitude forcing mechanisms along the east African margin across last glacial–interglacial transition. Quat. Sci. Rev. 125, 117–130. doi:10.1016/j.quascirev.2015.07.009

Chikaraishi, Y., Naraoka, H., 2003. Compound-specific δD–δ13C analyses of n-alkanes extracted from terrestrial and aquatic plants. Phytochemistry 63, 361–371. doi:10.1016/S0031-9422(02)00749-5

Collins, J.A., Schefuß, E., Mulitza, S., Prange, M., Werner, M., Tharammal, T., Paul, A., Wefer, G., 2013. Estimating the hydrogen isotopic composition of past precipitation using leaf-waxes from western Africa. Quat. Sci. Rev. 65, 88–101.

Collister, J.W., Rieley, G., Stern, B., Eglinton, G., Fry, B., 1994. Compound-specific δ 13C analyses of leaf lipids from plants with differing carbon dioxide metabolisms. Org. Geochem. 21, 619–627. doi:10.1016/0146-6380(94)90008-6

Compton, J.S., Herbert, C.T., Hoffman, M.T., Schneider, R.R., Stuut, J.-B., 2010. A tenfold increase in the Orange River mean Holocene mud flux: implications for soil erosion in South Africa. The Holocene 20, 115–122. doi:10.1177/0959683609348860

Compton, J.S., Maake, L., 2007. Source of the suspended load of the upper Orange River, South Africa. South African J. Geol. 110, 339–348. doi:10.2113/gssajg.110.2-3.339

Compton, J.S., Wiltshire, J.G., 2009. Terrigenous sediment export from the western margin of South Africa on glacial to interglacial cycles. Mar. Geol. 266, 212–222. doi:10.1016/j.margeo.2009.08.013

Cowling, R.M., Esler, K.J., Rundel, P.W., 1999. Namaqualand, South Africa – an overview of a unique winter-rainfall desert ecosystem. Plant Ecol. 142, 3–21. doi:10.1023/A:1009831308074

Cowling, R.M., Richardson, D.M., Pierce, S.M. (Eds.), 1997. Vegetation of Southern Africa. Cambridge University Press.

CSIR, 1988. Basic Physical Geography/Hydro Data for "Estuaries" of the Western Cape (CW 1-32). NRIO Data Report D8802.

DAFF (Department of Agriculture Forestry and Fisheries), 2016. Abstract of agricultural statistics. Department of Agriculture, Forestry and Fisheries, Pretoria, South Africa.

de Villiers, S., 2000. The strontium isotope systematics of the Orange River, Southern Africa. South African J. Geol. 103, 237–248. doi:10.2113/1030237

Desmet, P.G., 1996. The vegetation and restoration potential of the arid coastal belt between Port Nolloth and Alexander Bay, Namaqualand, South Africa.

Diefendorf, A.F., Freeman, K.H., Wing, S.L., Graham, H. V., 2011. Production of n-alkyl lipids in living plants and implications for the geologic past. Geochim. Cosmochim. Acta 75, 7472–7485. doi:10.1016/j.gca.2011.09.028

Dupont, L., Wyputta, U., 2003. Reconstructing pathways of aeolian pollen transport to the marine sediments along the coastline of SW Africa. Quat. Sci. Rev. 22, 157–174. doi:10.1016/S0277-3791(02)00032-X

Eglinton, G., Hamilton, R., 1967. Leaf epicuticular waxes. Science 156, 1322 – 1335.

Ehleringer, J.R., Phillips, S.L., Comstock, J.P., 1992. Seasonal variation in the carbon isotopic composition of desert plants. Funct. Ecol. 6, 396–404. doi:10.2307/2389277

Farmer, E.C., DeMenocal, P.B., Marchitto, T.M., 2005. Holocene and deglacial ocean temperature variability in the Benguela upwelling region: Implications for low-latitude atmospheric circulation. Paleoceanography 20. doi:10.1029/2004PA001049

Farquhar, G.D., Ehleringer, J.R., Hubick, K.T., 1989. Carbon Isotope Discrimination and Photosynthesis. Annu. Rev. Plant Physiol. Plant Mol. Biol. 40, 503–537. doi:10.1146/annurev.pp.40.060189.002443

Feakins, S.J., Sessions, A.L., 2010. Crassulacean acid metabolism influences D/H ratio of leaf wax in succulent plants. Org. Geochem. 41, 1269–1276.

Galy, V., Eglinton, T., France-Lanord, C., Sylva, S., 2011. The provenance of vegetation and environmental signatures encoded in vascular plant biomarkers carried by the Ganges–Brahmaputra rivers, Earth and Planetary Science Letters. doi:10.1016/j.epsl.2011.02.003

Gao, L., Guimond, J., Thomas, E., Huang, Y., 2015. Major trends in leaf wax abundance, δ2H and δ13C values along leaf venation in five species of C3 plants: Physiological and geochemical

implications. Org. Geochem. 78, 144–152. doi:10.1016/j.orggeochem.2014.11.005

Garcin, Y., Schefuß, E., Schwab, V.F., Garreta, V., Gleixner, G., Vincens, A., Todou, G., Séné, O., Onana, J.-M., Achoundong, G., Sachse, D., 2014. Reconstructing C3 and C4 vegetation cover using n-alkane carbon isotope ratios in recent lake sediments from Cameroon, Western Central Africa. Geochim. Cosmochim. Acta 142, 482–500. doi:10.1016/j.gca.2014.07.004

Garzanti, E., Andò, S., Padoan, M., Vezzoli, G., El Kammar, A., 2015. The modern Nile sediment system: Processes and products. Quat. Sci. Rev. 130, 9–56. doi:10.1016/j.quascirev.2015.07.011

Gray, C.E.D., 2009. Characterising the Namaqualand Mudbelt: Chronology, Palynology and Palaeoenvironments.

Gray, C.E.D., Meadows, M.E., Lee-Thorp, J.A., Rogers, J., 2000. Characterising the Namaqualand mudbelt of southern Africa: chronlogy, palynology and palaeoenvironments. South African Geogr. J. 82, 137–142. doi:10.1080/03736245.2000.9713705

Hahn, A., Compton, J.S., Meyer-Jacob, C., Kirsten, K.L., Lucasssen, F., Pérez Mayo, M., Schefuß, E., Zabel, M., 2015. Holocene paleo-climatic record from the South African Namaqualand mudbelt: A source to sink approach. Quat. Int. doi:10.1016/j.quaint.2015.10.017

Heinecken, T.J.E., 1981. Buffels (CW3), in: Heydorn, A.E.F., Grindley, T.J.E. (Eds.), Estuaries of the Cape. Part II: Synopses of Available Information on Individual Systems. CSIR Research Report 401, p. 32 pp.

Hemingway, J.D., Schefuß, E., Dinga, B.J., Pryer, H., Galy, V. V., 2016. Multiple plant-wax compounds record differential sources and ecosystem structure in large river catchments. Geochim. Cosmochim. Acta 184, 20–40. doi:10.1016/j.gca.2016.04.003

Herbert, C.T., Compton, J.S., 2007. Geochronology of Holocene sediments on the western margin of South Africa. South African J. Geol. 110, 327–338. doi:10.2113/gssajg.110.2-3.327

Hogg, A., Hua, Q., Blackwell, P.G., Niu, M., Buck, C.E., Guilderson, T.P., Heaton, T.J., Palmer, J.G., Reimer, P.J., Reimer, R.W., Turney, C.S.M., Zimmerman, S.R.H., 2013. SHCal13 Southern Hemisphere Calibration, 0–50,000 Years cal BP. Radiocarbon 55, 1889–1903. doi:10.2458/azu_js_rc.55.16783

Holmgren, K., Lee-Thorp, J.A., Cooper, G.R.J., Lundblad, K., Partridge, T.C., Scott, L., Sithaldeen, R., Siep Talma, A., Tyson, P.D., 2003. Persistent millennial-scale climatic variability over the past 25,000 years in Southern Africa. Quat. Sci. Rev. 22, 2311–2326.

Hou, J., D'Andrea, W.J., MacDonald, D., Huang, Y., 2007. Evidence for water use efficiency as an important factor in determining the δD values of tree leaf waxes. Org. Geochem. 38, 1251–1255. doi:10.1016/j.orggeochem.2007.03.011

Jurado, E., Dachs, J., Duarte, C.M., Simó, R., 2008. Atmospheric deposition of organic and black carbon to the global oceans. Atmos. Environ. 42, 7931–7939. doi:10.1016/j.atmosenv.2008.07.029

Just, J., Schefuß, E., Kuhlmann, H., Stuut, J.-B.W., Pätzold, J., 2014. Climate induced sub-basin

source-area shifts of Zambezi River sediments over the past 17ka. Palaeogeogr. Palaeoclimatol. Palaeoecol. 410, 190–199. doi:10.1016/j.palaeo.2014.05.045

Kolattukudy, P.E., 1970. Plant waxes. Lipids 5, 259–275. doi:10.1007/BF02532477

Kuechler, R.R., Schefuß, E., Beckmann, B., Dupont, L., Wefer, G., 2013. NW African hydrology and vegetation during the Last Glacial cycle reflected in plant-wax-specific hydrogen and carbon isotopes. Quat. Sci. Rev. 82, 56–67. doi:10.1016/j.quascirev.2013.10.013

Kuhn, T.K., Krull, E.S., Bowater, A., Grice, K., Gleixner, G., 2010. The occurrence of short chain n-alkanes with an even over odd predominance in higher plants and soils. Org. Geochem. 41, 88–95. doi:10.1016/j.orggeochem.2009.08.003

Le Roux, J.S., 1990. Spatial variations in the rate of fluvial erosion (sediment production) over South Africa. Water SA 16, 185–194.

Leduc, G., Herbert, C.T., Blanz, T., Martinez, P., Schneider, R., 2010. Contrasting evolution of sea surface temperature in the Benguela upwelling system under natural and anthropogenic climate forcings. Geophys. Res. Lett. 37, L20705. doi:10.1029/2010GL044353

Leithold, E.L., Blair, N.E., Wegmann, K.W., 2016. Source-to-sink sedimentary systems and global carbon burial: A river runs through it. Earth-Science Rev. 153, 30–42. doi:10.1016/j.earscirev.2015.10.011

Lim, S., Chase, B.M., Chevalier, M., Reimer, P.J., 2016. 50,000-years of vegetation and climate change in the Southern Namib Desert, Pella, South Africa. Palaeogeogr. Palaeoclimatol. Palaeoecol. doi:10.1016/j.palaeo.2016.03.001

Mabote, M.E., Rogers, J., Meadows, M.E., 1997. Sedimentology of terrigenous mud from the Orange River delta and the inner shelf off Namaqualand, South Africa. South African Geogr. J. 79, 108–114. doi:10.1080/03736245.1997.9713632

Meadows, M.E., Rogers, J., Lee-Thorp, J.A., Bateman, M.D., Dingle, R. V., 2002. Holocene geochronology of a continental-shelf mudbelt off southwestern Africa. The Holocene. doi:10.1191/0959683602hl521rp

Meyers, P.A., 1997. Organic geochemical proxies of paleoceanographic, paleolimnologic, and paleoclimatic processes. Org. Geochem. 27, 213–250. doi:10.1016/S0146-6380(97)00049-1

Meyers, P.A., 1994. Preservation of elemental and isotopic source identification of sedimentary organic matter. Chem. Geol. 114, 289–302. doi:10.1016/0009-2541(94)90059-0

Meyers, P.A., Ishiwatari, R., 1993. Lacustrine organic geochemistry—an overview of indicators of organic matter sources and diagenesis in lake sediments. Org. Geochem. 20, 867–900. doi:10.1016/0146-6380(93)90100-P

Mooney, H.A., Troughton, J.H., Berry, J.A., 1977. Carbon isotope ratio measurements of succulent plants in southern Africa. Oecologia 30, 295–305. doi:10.1007/BF00399762

Morant, P.D., 1984. Olifants (CW10), in: Heydorn, A.E.F., Grindley, T.J.E. (Eds.), Estuaries of the Cape. Part II: Synopses of Available Information on Individual Systems. CSIR Research Report 425.

Mucina, L., Rutherford, M., 2006. The vegetation of South Africa, Lesotho and Swaziland., in: The Vegetation of South Africa Lesotho and Sawziland. pp. 749–790. doi:10.1007/s

Nicholson, S.E., 1986. The nature of rainfall variability in Africa South of the Equator. J. Climatol. 6, 515–530. doi:10.1002/joc.3370060506

Pichevin, L., Cremer, M., Giraudeau, J., Bertrand, P., 2005. A 190 ky record of lithogenic grain-size on the Namibian slope: Forging a tight link between past wind-strength and coastal upwelling dynamics. Mar. Geol. 218, 81–96. doi:10.1016/j.margeo.2005.04.003

Prahl, F.., Ertel, J.., Goni, M.., Sparrow, M.., Eversmeyer, B., 1994. Terrestrial organic carbon contributions to sediments on the Washington margin. Geochim. Cosmochim. Acta 58, 3035–3048. doi:10.1016/0016-7037(94)90177-5

Prospero, J.M., Ginoux, P., Torres, O., Nicholson, S.E., Gill, T.E., 2002. Environmental characterization of global sources of atmospheric soil dust identified with the NIMBUS 7 Total Ozone Mapping Spectrometer (TOMS) absorbing aerosol product. Rev. Geophys. 40, 1002. doi:10.1029/2000RG000095

Rao, Z., Wu, Y., Zhu, Z., Jia, G., Henderson, A., 2011. Is the maximum carbon number of long-chain n-alkanes an indicator of grassland or forest? Evidence from surface soils and modern plants. Chinese Sci. Bull. 56, 1714–1720. doi:10.1007/s11434-011-4418-y

Richardson, D.M., 2000. Ecology and biogeography of Pinus. Cambridge University Press.

Rogers, J., Bremner, J.M., 1991. The Benguela Ecosystem. Part VII. Marine-Geological Aspects, in: Oceanography and Marine Biology: An Annual Review 29. pp. 1–85.

Rogers, J., Rau, A., 2006. Surficial sediments of the wave-dominated Orange River Delta and the adjacent continental margin off south-western Africa. African J. Mar. Sci. 28, 511–524. doi:10.2989/18142320609504202

Rommerskirchen, F., Eglinton, G., Dupont, L., Güntner, U., Wenzel, C., Rullkötter, J., 2003. A north to south transect of Holocene southeast Atlantic continental margin sediments: Relationship between aerosol transport and compound-specific δ 13 C land plant biomarker and pollen records. Geochemistry, Geophys. Geosystems 4, 1101–1128. doi:10.1029/2003GC000541

Rommerskirchen, F., Eglinton, G., Dupont, L., Rullkötter, J., 2006a. Glacial/interglacial changes in southern Africa: Compound-specific δ13C land plant biomarker and pollen records from southeast Atlantic continental margin sediments. Geochemistry, Geophys. Geosystems 7, Q08010. doi:10.1029/2005GC001223

Rommerskirchen, F., Plader, A., Eglinton, G., Chikaraishi, Y., Rullkötter, J., 2006b. Chemotaxonomic significance of distribution and stable carbon isotopic composition of long-chain alkanes and alkan-1-ols in C4 grass waxes. Org. Geochem. 37, 1303–1332. doi:10.1016/j.orggeochem.2005.12.013

Rooseboom, A., von Harmse, H.J., 1979. Changes in the sediment load of the Orange River during the period 1929-1969. IAHS - AISH Publ. 128, 459 – 470.

Schefuß, E., Kuhlmann, H., Mollenhauer, G., Prange, M., Pätzold, J., 2011. Forcing of wet phases

in southeast Africa over the past 17,000 years. Nature 480, 509–512.

Schefuß, E., Ratmeyer, V., Stuut, J.-B.W., Jansen, J.H.F., Sinninghe Damsté, J.S., 2003. Carbon isotope analyses of n-alkanes in dust from the lower atmosphere over the central eastern Atlantic. Geochim. Cosmochim. Acta 67, 1757–1767. doi:10.1016/S0016-7037(02)01414-X

Schlünz, B., Schneider, R.R., 2000. Transport of terrestrial organic carbon to the oceans by rivers: re-estimating flux- and burial rates. Int. J. Earth Sci. 88, 599–606. doi:10.1007/s005310050290

Schneider, R., Bleil, U., Buschhoff, H., Compton, J.S., Enneking, K., Frederichs, T., Herbert, C.T., Hessler, S., Hilgenfeldt, C., Kahle, G., Kim, J.-H., Machutchon, M., McMillan, I., Meyer-Schack, B., Ochsenhirt, W.-T., Rau, A.J., Rogers, J., Schacht, R., Schewe, F., Schnieders, L., Schulz, H.D., Spilker, S., Veitch, J., Weldeab, S., Wien, K., Wilke, I., Zahn, R., Zaric, S., Zatloukal, N., 2003. Cruise report M57/1. Berichte aus dem Fachbereich Geowissenschaften der Univ. Bremen.

Schwab, V.F., Garcin, Y., Sachse, D., Todou, G., Séné, O., Onana, J.-M., Achoundong, G., Gleixner, G., 2015. Effect of aridity on δ13C and δD values of C3 plant- and C4 graminoid-derived leaf wax lipids from soils along an environmental gradient in Cameroon (Western Central Africa). Org. Geochem. 78, 99–109. doi:10.1016/j.orggeochem.2014.09.007

Schwartz, H.I., 1969. Hydrologic aspects of limnology in South Africa. Hydrobiologia 34, 14–28. doi:10.1007/BF00040320

Scott, L., Marais, E., Brook, G.A., 2004. Fossil hyrax dung and evidence of Late Pleistocene and Holocene vegetation types in the Namib Desert. J. Quat. Sci. 19, 829–832. doi:10.1002/jqs.870

Scott, L., Neumann, F.H., Brook, G.A., Bousman, C.B., Norström, E., Metwally, A.A., 2012. Terrestrial fossil-pollen evidence of climate change during the last 26 thousand years in Southern Africa. Quat. Sci. Rev. 32, 100–118. doi:10.1016/j.quascirev.2011.11.010

Scott, L., Steenkamp, M., Beaumont, P.B., 1995. Palaeoenvironmental conditions in South Africa at the pleistocene-holocene transition. Quat. Sci. Rev. 14, 937–947. doi:10.1016/0277-3791(95)00072-0

Scott, L., Vogel, J.C., 2000. Evidence for environmental conditions during the last 20000 years in Southern Africa from 13C in fossil hyrax dung. Glob. Planet. Change 26, 207–215.

Shi, N., Schneider, R., Beug, H.-J., Dupont, L.M., 2001. Southeast trade wind variations during the last 135 kyr: evidence from pollen spectra in eastern South Atlantic sediments. Earth Planet. Sci. Lett. 187, 311–321. doi:10.1016/S0012-821X(01)00267-9

Simoneit, B.R.T., 1986. Characterization of Organic Constituents in Aerosols in Relation to Their rigin and Transport: A Review. Int. J. Environ. Anal. Chem. 23, 207–237. doi:10.1080/03067318608076446

Stuut, J.-B.W., Prins, M.A., Schneider, R.R., Weltje, G.J., Jansen, J.H.F., Postma, G., 2002. A 300-kyr record of aridity and wind strength in southwestern Africa: inferences from grain-size distributions of sediments on Walvis Ridge, SE Atlantic. Mar. Geol. 180, 221–233.

doi:10.1016/S0025-3227(01)00215-8

Taylor, A., 2004. A trace element study of sediments from the Olifants River estuary, the Berg River estuary, and the off-shore Mud Belt.

Tyson, P.D., 1986. Climatic change and variability in southern Africa.

Tyson, P.D., Preston-Whyte, R.A., 2000. The Weather and Climate of Southern Africa. Oxford University Press Southern Africa.

Urrego, D.H., Sánchez Goñi, M.F., Daniau, A.-L., Lechevrel, S., Hanquiez, V., 2015. Increased aridity in southwestern Africa during the warmest periods of the last interglacial. Clim. Past 11, 1417–1431. doi:10.5194/cp-11-1417-2015

van der Merwe, N.J., Medina, E., 1991. The canopy effect, carbon isotope ratios and foodwebs in amazonia. J. Archaeol. Sci. 18, 249–259. doi:10.1016/0305-4403(91)90064-V

Vogel, J.C., Fuls, A., Ellis, R.P., 1978. The geographical distribution of Kranz grasses in South Africa. S. Afr. J. Sci. 74, 209–215.

Vogts, A., Moossen, H., Rommerskirchen, F., Rullkötter, J., 2009. Distribution patterns and stable carbon isotopic composition of alkanes and alkan-1-ols from plant waxes of African rain forest and savanna C3 species. Org. Geochem. 40, 1037–1054. doi:10.1016/j.orggeochem.2009.07.011

Weldeab, S., Stuut, J.-B.W., Schneider, R.R., Siebel, W., 2013. Holocene climate variability in the Winter Rainfall Zone of South Africa. Clim. Past Discuss. 9, 2309–2356. doi:10.5194/cpd-9-2309-2013

Werger, M.J.A., Ellis, R.P., 1981. Photosynthetic pathways in the arid regions of South Africa. Flora 171, 64–75.

Woodward, J., Macklin, M., Fielding, L., Millar, I., Spencer, N., Welsby, D., 2015. Shifting sediment sources in the world's longest river: A strontium isotope record for the Holocene Nile. Quat. Sci. Rev. 130, 124–140. doi:10.1016/j.quascirev.2015.10.040

Zhao, X., Dupont, L., Meadows, M.E., Wefer, G., 2015. Pollen distribution in the marine surface sediments of the mudbelt along the west coast of South Africa. Quat. Int. doi:10.1016/j.quaint.2015.09.032